THE ASTROPHYSICAL JOURNAL SUPPLEMENT SERIES, 64:643–666, 1987 August

THE STRUCTURE OF BRIGHTEST CLUSTER MEMBERS. II. MERGERS

JAMES M. SCHOMBERT[1]
Palomar Observatory, California Institute of Technology; and Yale University Observatory
Received 1986 November 19; accepted 1987 January 8

ABSTRACT

Surface photometry of 342 bright elliptical galaxies in 103 clusters is analyzed for evidence of mergers. Structural differences between brightest cluster members (BCMs) and normal ellipticals can be summarized as having enlarged characteristic radii and shallow profile slopes ($\beta > -1.7$). Profile morphology criteria for the elliptical types gE, D, and cD are outlined. Comparison of observations with numerical simulations of mergers strongly suggests a past history of dynamical growth for BCMs. Weak correlations of global cluster properties to BCMs supports the hypothesis proposed by Merritt that mergers are important in early subgroups before virialization and the formation of a cluster identity.

Subject headings: galaxies: clustering — galaxies: photometry — galaxies: structure

I. INTRODUCTION

The centers of rich clusters are thought to be excellent laboratories for studies on the dynamical evolution of galaxies, for although the relative velocities are large (thus the time scale for interaction is small), the galaxy densities are high and the probability of interaction is greater than in the field. This will be particularly true when a large, dominant galaxy is located at the positional and kinematic center of the system and serves to enhance the effects of dynamical friction (Merritt 1985) or early in the life of a cluster when the components are grouped in small low-velocity subclusters with larger cross sections (Merritt 1984). In either case, the galaxies most likely to be affected by dynamical evolution are brightest cluster members (BCMs; a BCM is the first-ranked elliptical in a cluster, based on luminosity and size). Perhaps the strongest evidence for the dynamical evolution by mergers in BCMs to date is the study of Hoessel and Schneider (1985), which found 50% to have multiple nuclei, companions assumed to be in the process of accretion. On the other hand, the recent velocity studies by Tonry (1985) indicate that many of these nuclei are not in the process of merging but instead are on radial orbits passing through the center of the cluster (see Cowie and Hu 1986 for a dissenting view).

Galaxy interactions were first suggested by Holmberg (1940), and their disturbing effects on galaxy structure were supported from catalogs of interacting systems by Zwicky (1964) and the Arp Atlas of Peculiar Galaxies (Arp 1966), with its many examples of systems connected by thin bridges and tails. This interpretation lacked theoretical explanation until the numerical simulations of Toomre and Toomre (1972), which were able to reproduce similar structures using only gravity. A more severe interaction, either with a lower relative velocity or a smaller impact parameter, can lead to a resulting configuration which is bound (i.e., a merger) because of the transfer of orbital energy to internal dynamics and tidal features. An example of a recent event of this type is NGC 7252 (Schweizer 1982), where velocity information on the individual features strongly suggests an encounter leading to a merger. Encounters between ellipticals or between an elliptical and a disk system are not expected to form radial linear features, owing to the low rotation velocities in ellipticals. Instead, shell features, as cataloged by Malin and Carter (1983), are expected from the interactions of disks and ellipticals as demonstrated in the simulations of Quinn (1984). Numbers of interacting systems in galaxy catalogs plus estimates of the time scales of their features suggest that mergers are not rare events.

In studying the effects of mergers on galaxy structure, attention is immediately directed toward those galaxies known as the D/cD type (Matthews, Morgan, and Schmidt 1964; Morgan and Lesh 1965). Here exists a special class of objects distinguished by their diffuse appearance, extreme luminosities, and dominant central location in clusters. The philosophy that has always been extended to D/cD galaxies is that a special type of object requires a special process for its formation, and environmental effects appear to be the appropriate sort of process to explain all the observed features (Gunn and Tinsley 1976; Hausman and Ostriker 1978). Yet now a very different structural appearance is presented by BCMs when compared with interacting systems in the Arp atlas. In this case, the structure is smooth and concentric and, to first order, very similar to normal ellipticals rather than lumpy or distorted with tidal features. Of course, it is assumed that any linear or shell-like features that may have formed by interactions were later disrupted by the many close encounters with galaxies passing through the core. The main question to be addressed by this paper is whether the smooth luminosity profiles of BCMs differ from those of the other ellipticals and

[1]Visiting Astronomer, Cerro Tololo Inter-American Observatory, under contract with the National Science Foundation. Visiting Astronomer, Kitt Peak National Observatory, operated by the Association of Universities for Research in Astronomy, Inc., under contract with the National Science Foundation. Observations made with the Burrell Schmidt of the Warner and Swasey Observatories, Case Western Reserve University.

whether this difference can be explained by accretion and mergers.

The investigation of the structure of BCMs in this paper is a three-step process. The first step is to determine what are the exact parameters for the structure of a normal elliptical. This involves a question not only of analysis technique (i.e., what fitting function to use) but also of whether there exists an elliptical which is truly free of environmental effects (see § II). The second step is to identify major features which distinguish the morphological classes of gE-, D-, and cD-type galaxies (see § III*a*). The last step is to determine a procedure for quantifying the excess luminosity or structure of BCMs for comparison with simulation predictions of merger products (see §§ III*d* and III*e*).

This study is one of a long series of recent structural studies of BCMs (Strom and Strom 1978*a*, *b*, *c*, 1979; Hoessel, Gunn, and Thuan 1980; Thuan and Romanishin 1981; Malumuth and Kirshner 1985), and the data from these sources have been incorporated where appropriate. This series of papers has chosen to study the structure of elliptical galaxies over a range of environments in order to quantify the magnitude of dynamical growth on bright galaxies, but particular attention is given to those brightest cluster members in rich clusters, since they have the highest probability of unusual past histories. Paper I of this series (Schombert 1986) presented the data in the form of surface brightness profiles and outlined the analysis procedures and results to be used in this paper. The extension of the data sample with new observations and a summary of the data are presented in § II. Paper III of this series (Schombert 1987) will concern itself with cD envelopes and their properties.

II. OBSERVATIONS

a) *Sources*

Data for this study are derived from a variety of sources. Most of the profiles on cD galaxies are measured from photographic plates taken on wide-field telescopes in order to cover the full size of extended envelopes. The objects were selected to cover the fullest possible range of cluster environments and dynamical states as well as morphology type of the galaxies themselves. Cluster types were chosen using the Bautz-Morgan class (Bautz and Morgan 1970; Leir and van den Bergh 1977) and Rood-Sastry type (Struble and Rood 1986) as the primary criteria. Galaxy morphology was restricted so that all the galaxies were at least first-order ellipticals and among the top ten brightest in the cluster. This would include all D and cD galaxies; however, a few S0 galaxies were measured unknowingly. Peculiar ellipticals (i.e., ones with shells or low surface brightness features) were excluded from the sample in order to avoid the difficult interpretation of these complex structures. The original list of clusters as selected by Schombert (1984) is listed in Schombert (1986, hereafter Paper I), along with the source of the data. This data set has been supplemented by RCA CCD data taken on the Palomar 1.5 m telescope during the 1985–1986 observing season and reduced in the same manner outlined in Paper I. The old and new clusters are fully listed in Table 1 along with the source of the data. Many of the profiles used in Paper I were taken from the literature, in particular the sample of BCMs from the Michigan CCD system by Malumuth (1983), the photographic sample of poor clusters by Thuan and Romanishin (1981), and the original survey of cD galaxies by Oemler (1976) which is the progenitor of this study. Photometry for this study was taken in either the Johnson V or the Gunn g band (Thuan and Gunn 1976). Profiles range from an inner cutoff of 2 kpc down to surface brightnesses of 28–29 mag arcsec^{-2}. All magnitudes used below are in the V band, g-magnitudes are converted to V assuming $g - V = 0.18$ (Schneider 1982), typical for giant ellipticals. K-corrections as tabulated by Pence (1976) were also applied. Conversion to a linear scale (in kiloparsecs) and corrections for cosmological surface brightness dimming were made using the redshifts of Struble and Rood (1986), corrected for a Virgo infall of 300 km s^{-1}. An H_0 of 100 h km s^{-1} Mpc^{-1} and a q_0 of zero have been assumed (note that this differs from the value of $H_0 = 50$ used in Paper I). A complete tabulation of each profile or a figure of each galaxy would require more room than the journals currently allow. Hence, the reader is encouraged to write the author for a magnetic tape copy of the data sample.

b) *Fitting Functions*

Analysis of structure implies understanding surface photometry contours, which in turn means attempting to describe the shape of surface brightness profiles through the use of fitting functions. These functions are used to reduce the profile to two or three simple parameters, usually in terms of scale length and luminosity. Various methods of fitting surface brightness profiles were attempted in Paper I using the de Vaucouleurs $r^{1/4}$ law (de Vaucouleurs 1948), the exponential Hubble law (Oemler 1976), and King models (King 1966). However, none were completely successful in describing the shape of profiles for the full range of luminosity covered by this sample. The $r^{1/4}$ law was the most useful in describing the interior regions, but it often failed in the cores and in the regions of greatest interest for cD galaxies, the outer envelopes.

In particular, the $r^{1/4}$ law was found to be a good describer of structure only if the following conditions were met. The first was that the region of profile fitting be restricted to between 19 and 25 mag arcsec^{-2}. At the inner edge of a profile there is too much curvature because of the appearance of the core for a proper fit, and the outer regions usually had cutoffs or extended deviations from a $r^{1/4}$ fit (see below). The second condition is that the galaxy must be brighter than $M_V = -19$. At low luminosities, the $r^{1/4}$ law was completely inappropriate for the profiles in this sample, which are more like exponential Hubble or pure exponential profiles (see also Binggeli, Sandage, and Tarenghi 1984; Caldwell and Bothun 1986). On the other hand, it is surprising to find that even the more extreme BCMs, such as "nested" cD galaxies, usually have smooth $r^{1/4}$ profiles in their interiors. On the high-luminosity end of this sample almost all the galaxies have some middle region which is well described by an $r^{1/4}$ shape.

Much of the discussion section will also use isophotal properties, such as integrated magnitudes, $M(r)$, and surface brightnesses at particular radii, $\mu(r)$, in order to avoid the

TABLE 1

DATA SAMPLE AND SOURCES

Cluster	z	# of Galaxies	Telescope/ Source[a]	Emulsion	Filter
A42	0.1087	1	P60	...	Gunn g
A85	0.0499	3	P60	...	Gunn g
A115	0.1959	1	P60	...	Gunn g
A119	0.0446	1	P60	...	Gunn g
A150	0.0599	1	M	...	V
A151	0.0526	2	P60	...	Gunn g
A194	0.0178	2	P48	IIIa-J	WR4
A260	0.0348	1	P60	...	Gunn g
A262	0.0164	6	P48	IIIa-J	WR4
A358	0.0576	2	P60	...	Gunn g
A399	0.0714	1	P60	...	Gunn g
A400	0.0232	9	P48	103a-F	RG1
A401	0.0746	1	P60	...	Gunn g
A426(Perseus)	0.0183	14	O	...	V
A478	0.0900	1	P60	...	Gunn g
A496	0.0316	1	C	IIIa-J	GG385
A505	0.0540	1	M	...	V
A514	0.0697	3	P60	...	Gunn g
A539	0.0267	5	P48	IIIa-J	WR4
A569	0.0193	5	B	IIIa-J	GG385
A665	0.1816	4	P48	103a-F	RG1
A671	0.0497	5	B	IIIa-J	GG385
A779	0.0223	1	O	...	V
A957	0.0437	1	P60	...	Gunn g
A978	0.0527	5	B	IIIa-J	GG385
A993	0.0533	5	B	IIIa-J	GG385
A994	0.0390	1	M	...	V
A1126	0.0828	2	P60	...	Gunn g
A1139	0.0376	8	B	IIIa-J	GG385
A1177	0.0319	1	M	...	V
A1185	0.0349	8	B	IIIa-J	GG385
A1190	0.0794	2	P60	...	Gunn g
A1213	0.0469	4	B	IIIa-J	GG385
A1228	0.0344	4	P48	103a-F	RG1
A1238	0.0716	6	P60	...	Gunn g
A1314	0.0341	5	O	...	V
A1367	0.0213	8	P48	IIIa-J	WR4
A1383	0.0598	1	P60	...	Gunn g
A1413	0.1427	1	O	...	V
A1656(Coma)	0.0235	40	O	...	V
A1691	0.0722	1	P60	...	Gunn g
A1767	0.0756	2	P60	...	Gunn g
A1785	0.0792	1	P60	...	Gunn g
A1795	0.0620	1	P60	...	Gunn g
A1809	0.0788	3	P60	...	Gunn g
A1904	0.0714	1	M	...	V
A1913	0.0533	6	P60	...	Gunn g
A1983	0.043	6	B	IIIa-J	GG385
A1991	0.0589	1	P60	...	Gunn g
A2028	0.0772	1	P60	...	Gunn g
A2029	0.0767	1	M	...	V
A2052	0.0348	1	M	...	V
A2061	0.0768	3	P60	...	Gunn g
A2063	0.0337	3	P60	...	Gunn g
A2065(Cor Bol)	0.0721	2	B	IIIa-J	GG385
A2089	0.0743	1	P60	...	Gunn g
A2107	0.0425	1	M	...	V
A2124	0.0669	1	M	...	V
A2142	0.0903	2	P60	...	Gunn g
A2147	0.0357	1	M	...	V
A2151(Hercules)	0.0371	10	P48	IIIa-J	WR4
A2152	0.0383	3	P48	IIIa-J	WR4
A2162	0.0318	3	P48	103a-F	RG1
A2184	0.0546	1	P60	...	Gunn g
A2197	0.0303	3	P48	IIIa-J	GG385
A2199	0.0305	1	O	...	V
A2249	0.0808	3	P60	...	Gunn g

TABLE 1—*Continued*

Cluster	z	# of Galaxies	Telescope/ Source[a]	Emulsion	Filter
A2255	0.0769	3	P60	...	Gunn g
A2256	0.0601	3	P60	...	Gunn g
A2271	0.0616	1	P60	...	Gunn g
A2366	0.0542	1	M	...	V
A2400	0.0881	2	P60	...	Gunn g
A2420	0.0823	2	P60	...	Gunn g
A2440	0.0573	3	P60	...	Gunn g
A2457	0.0595	1	M	...	V
A2469	0.0656	1	P60	...	Gunn g
A2572	0.0395	2	P48	IIIa-J	WR4
A2589	0.0420	1	M	...	V
A2593	0.0440	4	P60	...	Gunn g
A2634	0.0322	4	P48	IIIa-J	WR4
A2666	0.0273	1	O	...	V
A2670	0.0749	1	O	...	V
A2700	0.0978	1	P60	...	Gunn g
Virgo	0.0046	5	P48	IIIa-J	WR4
CA0340-538	0.0578	2	C	IIIa-J	GG385
DC0107-46	0.023	2	C	IIIa-J	GG385
SC1325-31	0.0466	11	U	...	...
SC1328-32	0.0434	7	U	...	...
SC1331-31	0.0488	2	U	...	...
Centaurus	0.0104	2	C	IIIa-J	GG385
Fornax	0.0051	7	C	IIIa-J	GG385
AWM 1	0.0265	1	TR	...	Gunn g
AWM 2	0.0223	1	M	...	V
AWM 3	0.0152	1	M	...	V
AWM 4	0.0307	1	TR	...	Gunn g
AWM 5	0.0342	1	TR	...	Gunn g
AWM 6	0.0357	1	M	...	V
AWM 7	0.0182	1	TR	...	Gunn g
MKW 1s	0.0158	1	TR	...	Gunn g
MKW 2	0.0291	1	TR	...	Gunn g
MKW 4	0.0186	1	TR	...	Gunn g
MKW 5	0.0238	1	TR	...	Gunn g
MKW 9	0.0376	1	TR	...	Gunn g

NOTE.—Redshifts are from Struble and Rood 1986 and above sources, corrected for a 30 km s^{-1} Virgo infall.

[a]P60 = Palomar 60 inch (1.5 m) CCD; P48 = Palomar Schmidt; B = Case Western Reserve University Burrell Schmidt; C = CTIO Michigan Schmidt; U = UK/SERC Southern Sky Survey; O = Oemler 1976; TR = Thuan and Romanishin 1981; M = Malumuth 1983.

bias from fitting functions. These parameters are derived directly from the profiles themselves, rather than from aperture photometry, and thus have the advantage of avoiding complications due to multiple nuclei and ellipticity corrections. King models were fitted to all the BCMs in this study; some galaxies are well fitted by King models, but in most cases BCMs are not well described by these types of configurations.

c) *Templates*

One useful procedure, especially in distinguishing cD from D galaxies, was to construct template profiles from the normal ellipticals of this sample (i.e., all non–first-ranked galaxies). Empirical evidence of a trend of structure with luminosity and justification for building templates comes from an inspection of Figure 7 in Paper I. By the technique of interpolating radius-radius plots described in Paper I, templates were determined for the luminosity range -17 to -22.5 and are presented in Figure 1 in both log radius space and $r^{1/4}$ space for comparison with $r^{1/4}$ fits, which are, of course, straight lines in this coordinate system. The high-luminosity end was strongly weighted toward isolated ellipticals in order to free the templates of environmental effects. However, no evidence of difference in structure between cluster and field ellipticals was seen in plots of luminosity versus characteristic radius. The templates describe the expected trend of increasing size with increasing luminosity, and also display an increase in inner surface brightness and decrease in profile slope. These templates are also most useful for determining the amount of excess light associated with cD envelopes (see Paper III of this series).

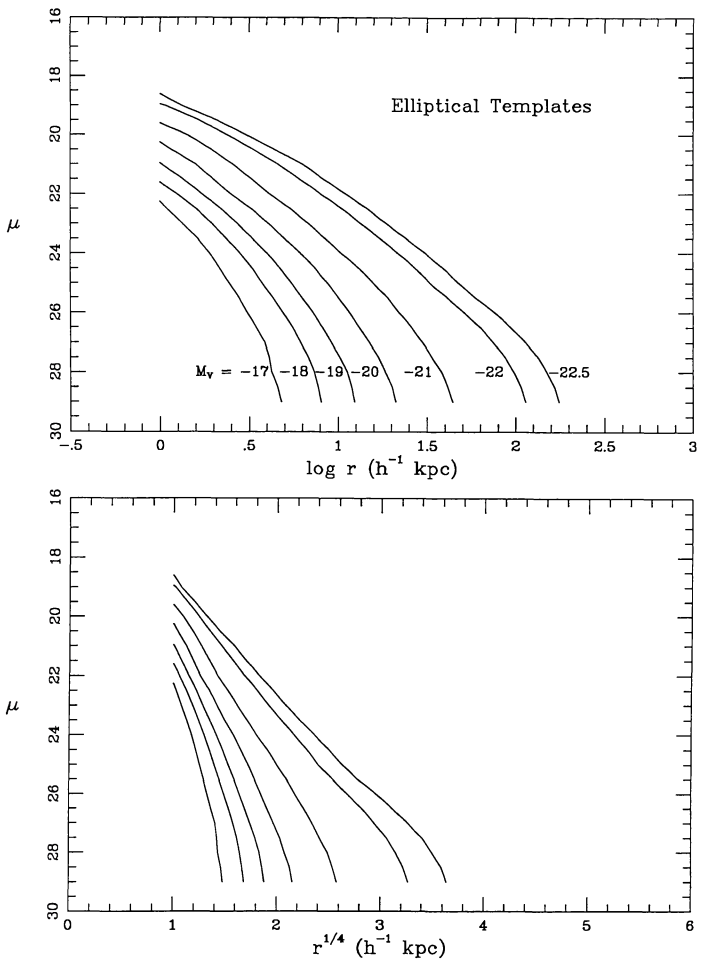

FIG. 1.—Elliptical template profiles for the luminosity range of this sample. The templates are plotted in log r and $r^{1/4}$ space for comparison with Fig. 2 and the data from Paper I. Each profile is marked with corresponding 16 kpc aperture magnitude. The construction technique was outlined in Paper I.

III. DISCUSSION

a) *Profile Morphology*

There is a great deal of confusion in the literature over the exact meaning of the classifications gE, D, and cD. Historically, the categories were chosen to classify the change in size and average surface brightness based on visual inspection of photographic plates. With respect to the profiles in this sample, it is possible to define the three categories only on the basis of the appearance of the surface brightness profiles.

Normal ellipticals can be defined from the sequence of templates constructed in Paper I. Since these templates are drawn from a range of environments, it is not possible to determine small deviations in structure from cluster to cluster in this sample (see Strom and Strom 1979). Each galaxy must be taken as an individual, but on average a normal elliptical is one with a power-law slope [$I(r) \propto r^{\beta}$] of $\beta < -1.7$ and a profile cutoff around 26–27 mag arcsec^{-2}. The high-luminosity end of normal ellipticals would be the giant ellipticals or gE galaxies, typified by their large size (Holmberg radii > 50 kpc) and $r^{1/4}$ profile shapes. Many of the gE galaxies have a slight distention of the outer envelope reminiscent of the Kormendy T3 objects (Kormendy 1977). However, no correlation between this feature and close companions has been found, and the distention appears to be a normal component of high-luminosity ellipticals. The bright cluster ellipticals have similar luminosity counterparts in the field (e.g., NGC 4014 and NGC 1339.5+2638).

The D galaxies are typified by their large, diffuse appearance. In terms of structure these correspond to profiles which have larger effective radii than normal ellipticals of similar luminosity. They also have shallower profile slopes than gE galaxies (Malumuth 1983) with slopes from −1.7 to −1.2. They are always quite large (Holmberg radii > 50 kpc) and are often one of the top three brightest galaxies in a cluster residing at the kinematic and density centers of clusters (Beers and Geller 1983; Quintana and Lawrie 1982). They all have $r^{1/4}$-type profiles. Operationally, a D galaxy will be defined using the above slopes and sizes only, not cluster position.

The cD galaxies have all the properties of D galaxies, with one addition, a large extended envelope (Oemler 1976). These envelopes form at a distinct break in the profile, usually between 24 and 25 mag arcsec^{-2}, and often have outer radii

TABLE 2

SUMMARY OF ELLIPTICAL CLASSES

Type	Profile Shape	β	r_H (kpc)	Location
gE	$r^{1/4}$	-1.9 to -1.7	50–100	Field, cluster cores
D	$r^{1/4}$, shallow	-1.7 to -1.2	50–130	Cluster peaks only
cD ...	$r^{1/4}$, shallow, extended envelope	-1.7 to -1.2	80–300	Cluster peaks only

in excess of 500 kpc. Despite the presence of satellite companions embedded in many cD galaxies, the inner profiles are usually $r^{1/4}$ in shape, although diffuse like D galaxies. From the above criteria, the poor-cluster cD galaxies of Thuan and Romanishin (1981) fall into the D class. The three types of systems are summarized in Table 2, with examples in Figure 2. A list of each galaxy in this sample and its classification based on profile shape can be found in Table 3. Also found in Table 3 are $M_{16\ \mathrm{kpc}}$, luminosity inside the 16 kpc radius; $\mu_{2\ \mathrm{kpc}}$, surface brightness at 2 kpc; log r_e, the effective radius in kiloparsecs from $r^{1/4}$ fits; μ_e, the effective surface brightness; β, the profile slope; and log r_H, the Holmberg radius for each galaxy. Poor $r^{1/4}$ fits are indicated.

The relation between BCMs and D/cD galaxies is not clearly defined when profile type is considered. In this study 74 galaxies had profile slopes less than -1.7 (a first-order D or cD galaxy); of these, 67 (91%) were BCMs. At least one cD (NGC 6034 in Hercules) is not a BCM; however, it is the dominant member of a local subcluster. In the cases where a galaxy was classed D/cD yet was not a BCM, the BCMs in those clusters were always of the D or cD type. The cluster morphology confuses this point, since each subcluster in an irregular system should be considered as a separate cluster with a particular history of its own, hence the concept of BCM blurs.

Since galaxy classification is usually done by visual inspection of photographic plates, there is confusion between D and cD galaxies owing to the fact that the eye does not detect faint envelopes but rather is measuring some quantity which is related to size and slope of the profile (Malumuth 1983). For comparison, in Figure 3 is plotted the profile classification from Table 3 as a function of the visual classifications made by Struble and Rood (1986) from the Palomar Sky Survey. There is no distinction between D and cD galaxies in their scheme; however, there is also no tendency for galaxies with extended envelopes to be distinguished from diffuse ellipticals, as can be seen by the equal numbers of D and cD that were classified as cD. D and cD galaxies were more often confused with S0 galaxies than were normal galaxies. A good example of cD versus D galaxy classification is the central galaxy in A2029 (IC 1101), which was classified by both Struble and Rood and Dressler (1976) as a cD, yet its profile shows no evidence of an extended envelope characteristic of cD galaxies A1413 and A2670. The extreme size (Holmberg radius = 120 kpc) and very shallow profile slope ($\beta = -1.49$) seem responsible for this misclassification. There is also an occasional S0 in the D sample, as demonstrated by A1177, a cD galaxy listed by Struble and Rood which nevertheless has the distinctive bulge and disk profile shape of an S0. A distinction between cD galaxies and S0's can be drawn by considering the scale of cD's and the fact that cD envelopes break from the profile at fainter levels than S0 disks.

b) *General Structure*

The $r^{1/4}$ law is the easiest to interpret, since it contains only two parameters, scale length and characteristic surface brightness. However, because of its limited nature, deviations from $r^{1/4}$ law can be described only in a qualitative fashion. Figure 2 presents several examples of good and bad $r^{1/4}$ fits for the morphological classes discussed above. The failure of the $r^{1/4}$ fits for low-luminosity ellipticals is best seen in Figure 2*a*, containing RB 31, which has an $M_V = -17.7$ (see also Binggeli, Sandage, and Tarenghi 1984). Note the good $r^{1/4}$ fits of cD galaxies until the point where the extended envelopes break from the profiles.

The best-fit $r^{1/4}$-law parameters are listed in Table 3, along with a note indicating the quality of the fit (a "poor fit" meaning that the galaxy was simply *not* $r^{1/4}$). The (μ_e, log r_e)-diagram is shown in Figure 4, along with the relation from Kormendy (1980) corrected for a Virgo infall of 300 km s^{-1}. A least-squares fit to the data did not produce significantly different values from previous studies. The large scatter around this relation exceeds the error bars of the fits and indicates that, even with the above fitting restrictions, ellipticals are not $r^{1/4}$ as a class of objects (see also Djorgovski 1985).

c) *BCM Structure*

BCMs are known to have special properties with respect to other bright ellipticals. By definition, they represent the extreme end of the luminosity function with an unusually narrow dispersion in luminosity, and average luminosities in excess of a simple extrapolation of the cluster luminosity function (Sandage 1973; Schneider 1982). They are often at the centers of clusters, both in galaxy density maps and X-ray contours (Beers and Geller 1983; Forman and Jones 1982). First-ranked galaxies are known to have more than their fair share of companion galaxies (Hoessel and Schneider 1985) but are missing any slow-moving companions (Tonry 1985; for a dissenting view see Cowie and Hu 1986). They are often highly flattened (Sastry 1968; Schombert 1986) and aligned with the cluster (Binggeli 1982). Previous studies on the structure of BCMs have noted their extreme size and luminosity plus the fact that their cores are brighter than those of normal ellipticals (Oemler 1976; Hoessel, Gunn, and Thuan 1980), yet there has been little direct evidence for any structural difference between BCMs and other ellipticals. However,

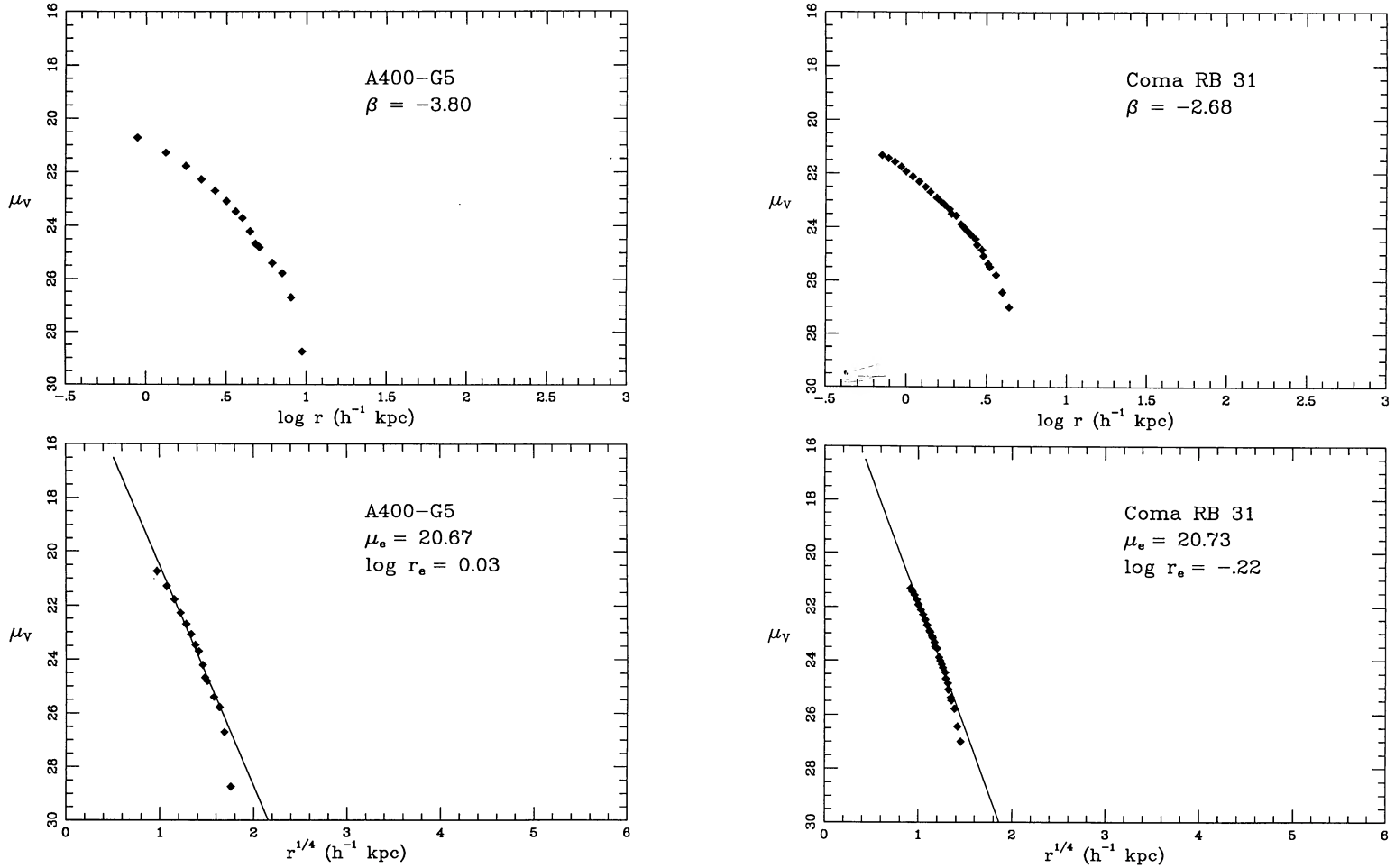

FIG. 2*a*.—Examples of two low-luminosity ellipticals, A400−G5 and RB 31 in Coma. Best $r^{1/4}$ fits are shown. None of the ellipticals in this sample below $M_V = -19$ were well fitted with the $r^{1/4}$ law.

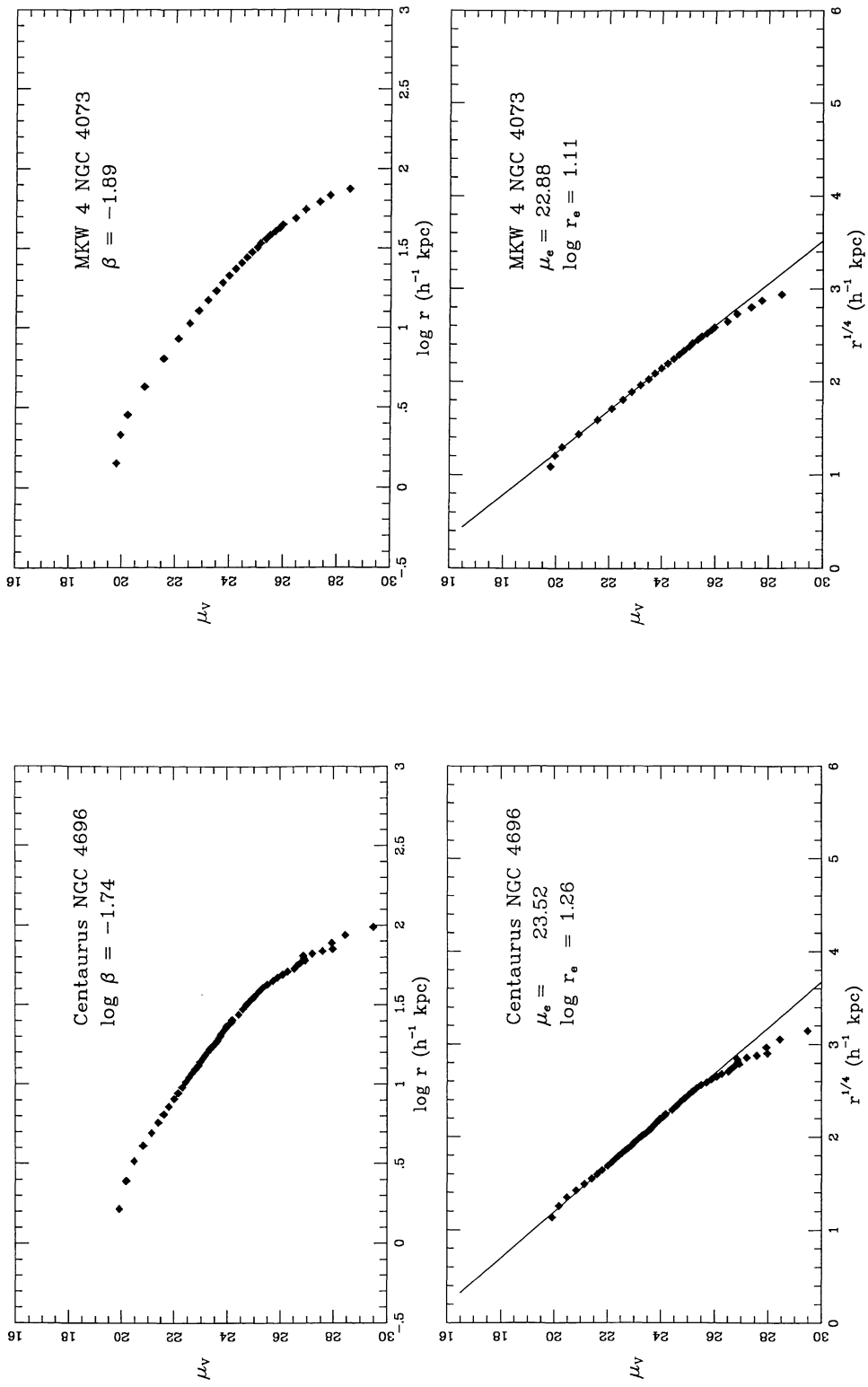

FIG. 2*b*.—Examples of two giant ellipticals (gE), NGC 4696 in Centaurus and NGC 4073 in MKW 4. Best $r^{1/4}$ fits are shown. Objects of this class are well fitted by the templates in Fig. 1 and have Holmberg radii > 50 kpc. The middle sections of their profiles are good $r^{1/4}$ regions with average profile slopes of $\beta = -1.7$ to -1.9.

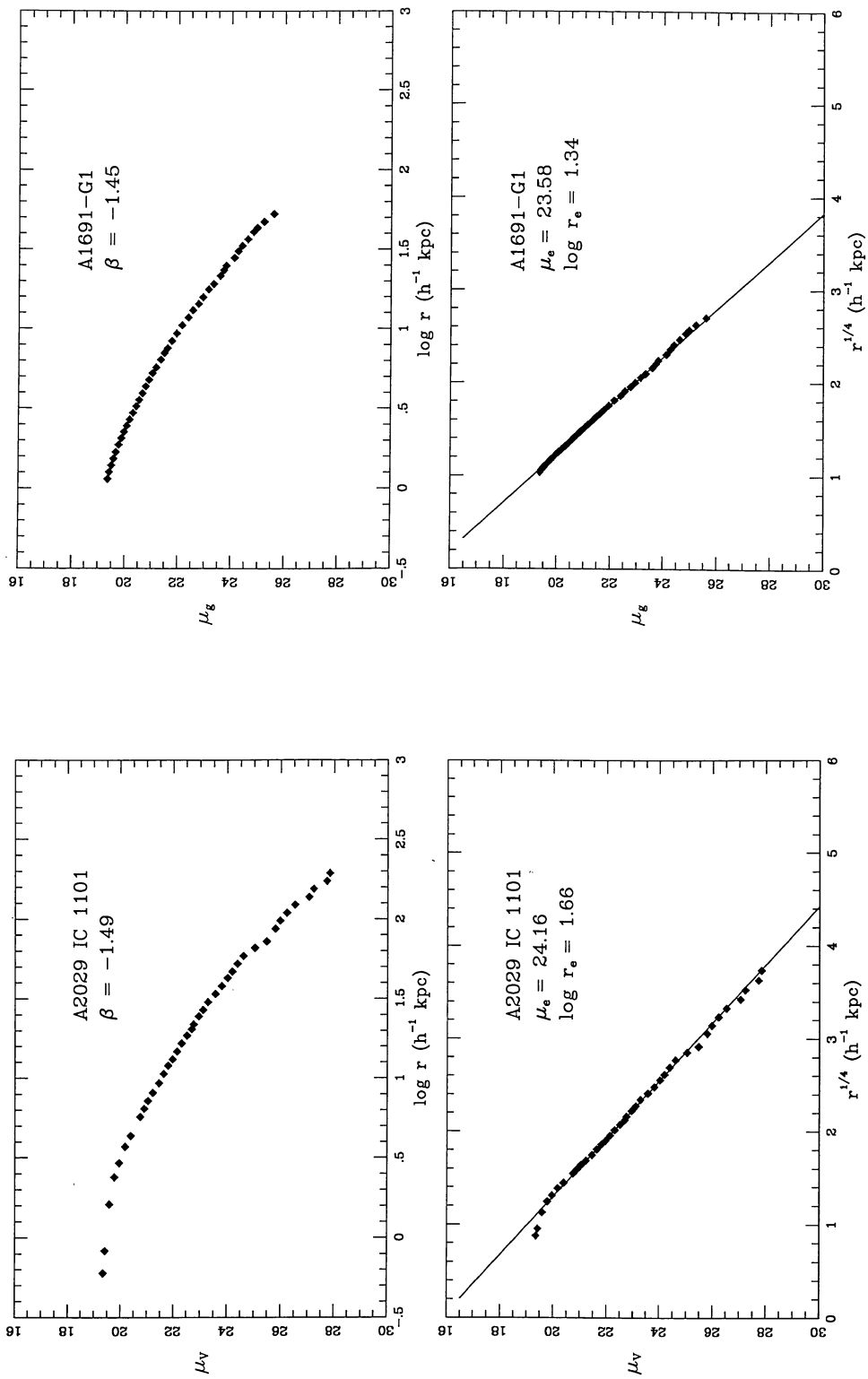

FIG. 2c.—Examples of galaxies IC 1101 in A2029 and A1691 – G1. Best $r^{1/4}$ fits are shown. This class of objects is typified by Holmberg radii > 50 kpc and shallow profile slopes ($\beta < -1.7$). The middle sections of their profiles are good $r^{1/4}$ regions. D and cD types are separated by the presence of extended envelopes.

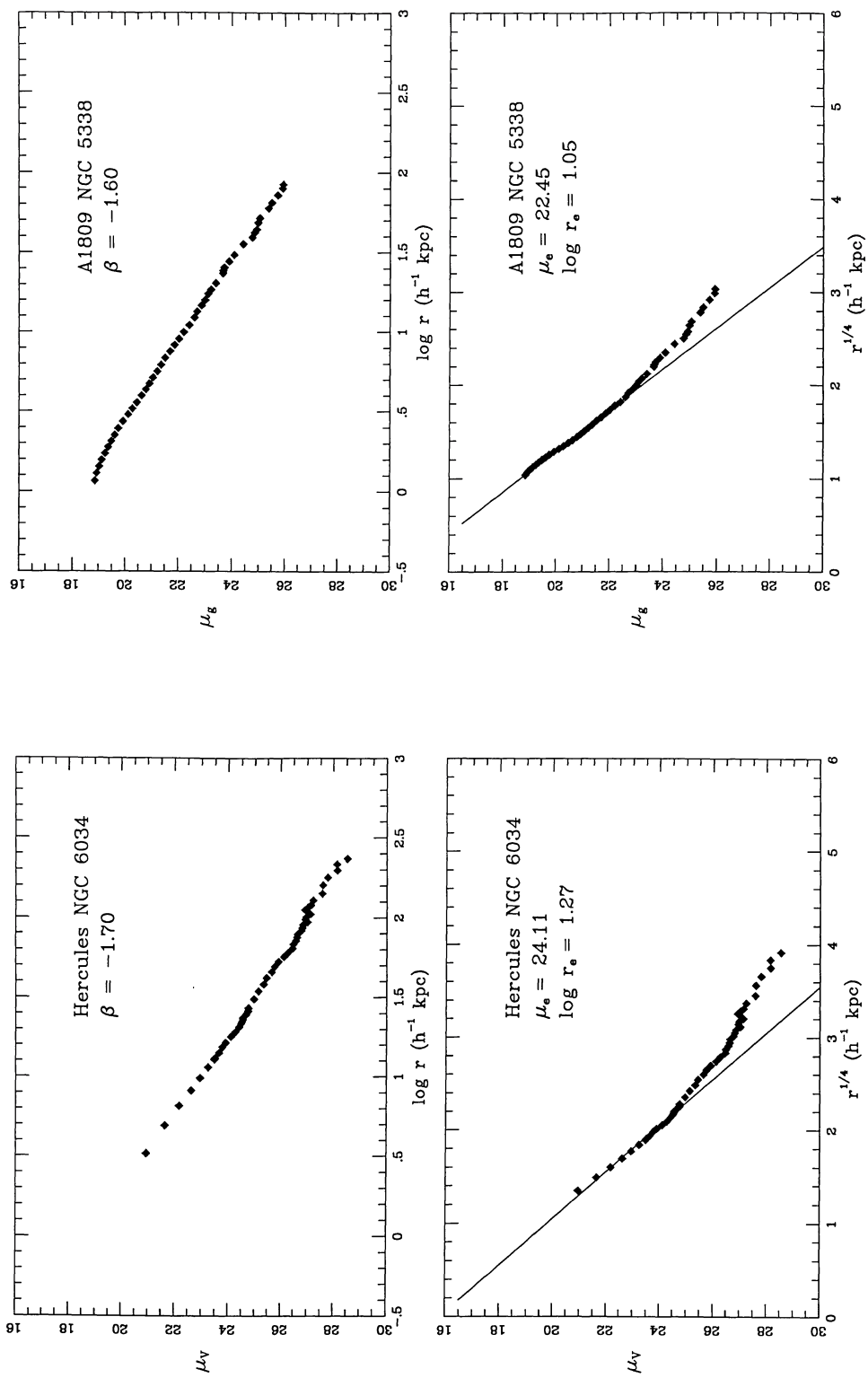

FIG. 2*d*.—Examples of cD galaxies NGC 6034 in Hercules and NGC 5338 in A1809. Best $r^{1/4}$ fits are shown. Galaxies of cD type have all the characteristics of D galaxies with the addition of large extended envelopes, often with outer radii on the order of 1–2 Mpc.

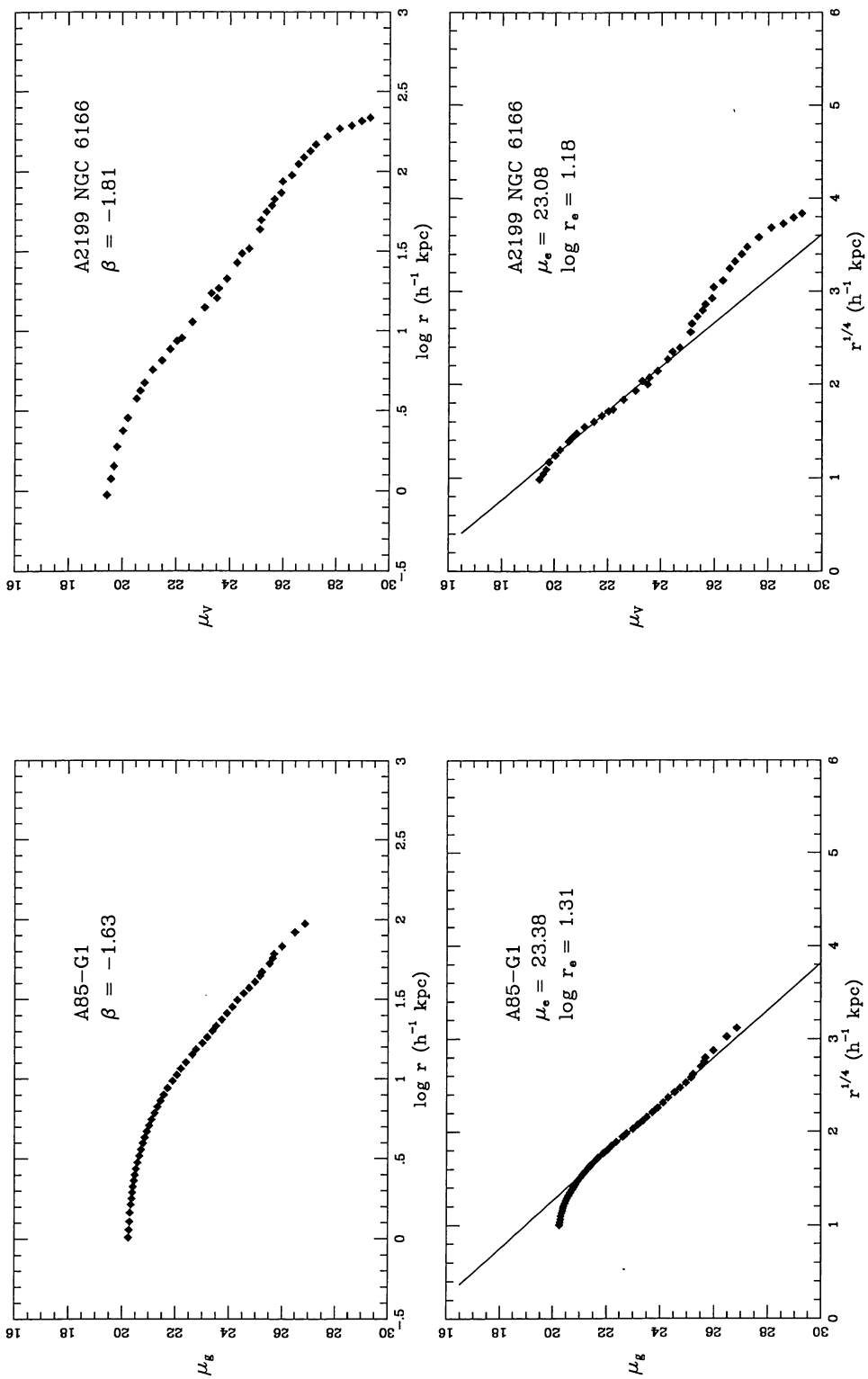

FIG. 2*e*.—Examples of low central surface brightness D and cD galaxies A85 – Gi and NGC 6166 in A2199. Best $r^{1/4}$ fits are shown. These systems are abnormal in their highly depressed central regions (see for comparison NGC 5338 in Fig. 2*d*). Both objects also display unusual emission features in their spectra.

TABLE 3

STRUCTURAL PARAMETERS

Cluster	Galaxy	type	M_{16kpc}	μ_{2kpc}	log r_e	μ_e	β	log r_H
A42	G1	D	−22.40	20.41	1.66	24.73	−1.25	1.80
A85	G1	D/cD[a]	−22.27	20.39	1.31	23.38	−1.63	1.92
	G2	E	−21.48	20.44	1.10	23.55	−1.53	1.64
	G3	E	−21.08	20.52	0.62	21.90	−1.83	1.38
A115	G1	E	−23.17	19.79	1.14	22.40	−1.79	1.66
A119	UGC 579	D	−22.15	19.99	1.40	23.93	−1.34	1.76
A150	UGC 716	cD	−22.14	19.96	1.39	24.14	−1.58	2.00
A151	G1	cD	−22.35	19.87	1.46	23.98	−1.37	2.02
	G2	E	−21.36	20.28	0.68	21.91	−1.87	1.47
A194	NGC 547	gE	−22.28	19.71	1.11	22.76	−1.93	1.81
	NGC 564	E	−21.10	20.70	0.84	22.76	−1.99	1.55
A260	IC 1733	D	−21.92	19.90	1.04	22.81	−1.58	1.74
A262	NGC 708	D	−21.62	20.22	1.29[b]	24.16	−1.59	1.73
	NGC 679	E	−21.32	20.03	0.62	21.69	−2.12	1.44
	NGC 687	E	−21.31	20.06	0.58	21.48	−2.26	1.47
	NGC 759	E	−21.00	20.30	0.50	21.37	−2.34	1.32
	IC 171	E	−21.59	19.90	0.77	22.10	−2.09	1.55
	UGC 1308	cD	−21.60	19.88	0.93	22.80	−1.47	1.94
A358	G1	cD	−22.13	19.83	1.25	23.45	−1.53	2.02
	G2	S0	−21.46	20.30	0.99[b]	23.17	−1.64	1.29
A399	UGC 2438	D	−22.10	20.53	1.69	25.00	−1.20	1.79
A400	G1	cD[c]	−21.31	20.61	1.15	24.04	−1.49	1.80
	G2	E	−21.02	20.48	0.76	22.67	−1.97	1.41
	G3	E	−20.46	21.07	0.70	22.96	−2.05	1.32
	G4	E	−19.89	21.59	0.54	22.85	−2.11	1.24
	G5	E	−19.15	21.86	0.03	20.67	−3.80	0.91
	G6	E	−19.27	22.09	0.69	23.94	−2.01	1.04
	G7	E	−19.25	22.06	0.21	21.71	−3.29	1.01
	G8	E	−19.63	21.55	0.01	20.14	−2.75	1.07
	G9	E	−19.12	22.20	0.42	22.93	−2.53	1.07
A401	UGC 2450	D	−22.24	20.24	1.67	25.00	−1.23	1.92
Perseus	NGC 1275	cD	−22.22	19.34	1.03	22.59	−1.80	1.94
	NGC 1265	E	−21.88	19.66	0.84	22.11	−2.01	1.55
	NGC 1270	E	−20.95	20.31	0.30	20.46	−2.58	1.19
	NGC 1272	S0/E	−21.16	20.83	1.21[b]	24.37	−1.55	1.55
	NGC 1273	E	−20.64	20.69	0.37	21.14	−2.55	1.29
	NGC 1278	E	−21.19	20.29	0.68	22.04	−2.18	1.32
	NGC 1282	E	−20.72	20.74	0.56	22.05	−2.13	1.30
	NGC 1283	E	−19.66	21.75	0.32	21.95	−2.54	1.14
	NGC 1293	E	−20.81	20.52	0.44	21.38	−2.16	1.41
Perseus	IC 310	E	−21.16	20.44	0.76	22.51	−2.07	1.49
	10	E	−19.35	22.12	0.32	22.34	−2.24	1.09
	11	E	−19.24	21.84	0.13	21.18	−2.30	0.97
	0314.6+1416	E	−19.43	21.82	0.18	21.42	−2.42	1.02
	0316.2+4127	E	−20.11	21.01	0.31	21.29	−2.27	1.09
A478	G1	D	−21.02	21.61	1.55	25.69	−1.18	1.75
A496	G1	D	−22.07	20.08	1.49	24.44	−1.48	1.88
A505	UGC 3197	D	−22.64	19.46	1.38	23.38	−1.38	2.00
A514	G1	E	−22.05	19.73	0.89	22.14	−1.82	1.61
	G2	S0	−21.46	20.22	0.86[b]	22.63	−1.76	1.57
	G3	E	−21.75	20.04	0.87	22.33	−1.81	1.58
A539	UGC 3274	D	−21.62	20.29	1.44	24.70	−1.47	1.96
	ZW421019	E	−21.64	20.06	0.91	22.77	−1.85	1.60
	G4	E	−20.62	20.89	0.58	22.41	−2.03	1.37
	G5	E	−20.01	21.15	0.16	20.61	−2.75	1.15
	G7	E	−20.61	20.55	0.18	20.18	−2.70	1.16
A569	NGC 2329	E	−21.76	19.79	0.80	22.07	−2.12	1.56
	UGC 3696	E	−21.19	20.19	0.54	21.49	−2.21	1.48
	G3	E	−20.73	20.64	0.60	22.18	−2.16	1.23
	G4	E	−20.28	20.64	−0.06	18.92	−3.56	1.08
	G7	E	−19.94	21.37	0.38	21.85	−2.44	1.10
A665	G1	D	−22.74	20.00	1.58	24.62	−1.51	1.85
	G2	E	−22.28	20.01	0.89	22.56	−2.03	1.54
	G3	E	−22.17	20.27	1.15	23.70	−1.76	1.63
	G5	E	−21.96	20.77	1.29	24.44	−1.69	1.52
A671	IC 2378	D	−22.50	19.64	1.44	23.88	−1.60	1.79
	G2	E	−22.03	19.81	0.93	22.47	−1.99	1.69
	G3	E	−21.58	20.04	0.59	21.30	−2.33	1.45
	G4	E	−21.21	20.51	0.75	22.46	−2.10	1.46
	G5	E	−21.81	19.86	0.88	22.52	−1.96	1.55
A779	NGC 2832	cD:[d]	−22.11	19.70	1.05	22.79	−1.47	1.69
A957	UGC 5515	D	−22.20	19.90	1.41	23.85	−1.45	1.94
A978	G1	D	−22.24	19.76	1.34	23.86	−1.64	1.82
	G2	E	−21.27	20.27	0.62	21.81	−2.24	1.32
	G3	E	−21.20	20.40	0.64	21.96	−2.25	1.31
	G4	E	−21.31	20.34	0.80	22.65	−1.97	1.53
	G5	E	−20.87	20.60	0.33	20.52	−2.69	1.24
A993	G1	gE	−22.31	19.62	0.94	22.18	−2.07	1.76
	G2	gE	−22.16	19.76	0.92	22.24	−2.06	1.73
	G3	E	−22.12	19.72	1.06	22.94	−1.86	1.68

TABLE 3—*Continued*

Cluster	Galaxy	type	M_{16kpc}	μ_{2kpc}	log r_e	μ_e	β	log r_H
A993	G5	E	−21.67	20.10	0.93	22.83	−1.94	1.83
	G6	E	−21.40	20.22	0.76	22.37	−2.01	1.52
A994	G1	E	−21.94	19.66	0.75	21.78	−2.08	1.51
A1126	G1	D	−22.77	19.81	1.29	22.97	−1.59	1.89
	G2	S0	−21.74	20.38	1.24[b]	23.94	−1.38	1.61
A1139	UGC 6057	E	−21.07	20.76	1.17	24.33	−1.62	1.65
	UGC 6067	E	−20.47	21.18	0.83	23.53	−1.95	1.39
	G3	E	−20.63	20.99	0.72	22.85	−2.17	1.38
	G4	E	−20.41	21.02	0.63	22.65	−2.10	1.33
	G5	E	−20.49	21.06	0.73	23.08	−2.03	1.39
	G6	E	−20.07	21.33	0.58	22.78	−2.12	1.28
	G7	E	−20.25	21.24	0.64	22.90	−2.14	1.41
	G8	E	−20.39	21.26	0.77[b]	23.26	−2.21	1.21
A1177	UGC 6203	S0	−22.18	19.85	1.36	23.89	−1.46	1.75
A1185	NGC 3550	S0	−21.35	20.60	1.02	23.44	−1.99	1.65
	NGC 3553	E	−20.52	21.02	0.72	22.95	−2.08	1.47
	NGC 3554	E	−20.27	21.16	0.60	22.67	−2.14	1.32
	NGC 3558	E	−20.84	20.82	0.90	23.49	−1.85	1.52
	NGC 3561	E	−20.82	21.04	1.07	24.15	−1.74	1.50
	UGC 6218	E	−20.38	21.15	0.67	22.84	−2.15	1.38
	G7	E	−20.69	20.83	0.66	22.56	−2.15	1.33
	G8	E	−19.92	21.47	0.52	22.68	−2.14	1.35
A1190	G1	D	−22.25	20.10	1.31	23.62	−1.43	1.81
	G2	gE	−22.14	19.77	1.11	23.03	−1.68	1.81
A1213	UGC 6292	E	−21.16	20.59	0.83	22.84	−2.02	1.51
	G2	E	−21.09	20.62	0.67	22.13	−2.21	1.40
	G4	E	−20.88	20.75	0.71	22.57	−2.10	1.44
	G6	E	−20.39	21.13	0.48	21.85	−2.43	1.27
A1228	IC 2738	E	−21.27	20.24	0.71	22.21	−2.06	1.41
	IC 2744	E	−21.20	20.41	0.91	23.19	−1.81	1.55
	UGC 6394	E	−21.82	20.06	1.05	23.12	−1.84	1.65
	G4	E	−21.00	20.49	0.63	22.07	−2.29	1.32
A1238	G1	cD	−21.85	20.23	0.75	22.15	−1.48	1.86
	G2	E	−21.12	20.37	0.53	21.41	−1.73	1.26
	G3	E	−20.75	20.65	0.43	21.24	−1.97	1.14
	G4	E	−20.79	20.69	0.54	21.79	−1.91	1.19
	G5	E	−21.10	20.55	0.68	22.22	−1.89	1.36
	G6	E	−20.63	20.82	0.51	21.77	−1.84	1.14
A1314	IC 708	E	−21.95	19.67	0.93	22.55	−1.88	1.63
	IC 709	E	−22.39	19.03	0.72	21.17	−2.08	1.55
	IC 711	E	−21.32	20.16	0.56	21.47	−2.17	1.46
	1133.8+4920	E	−21.48	20.03	0.62	21.58	−2.18	1.45
	1133.9+4920	E	−21.21	20.22	0.51	21.36	−2.17	1.34
A1367	NGC 3842	gE	−21.96	19.67	1.04	22.89	−1.85	1.76
	NGC 3837	E	−20.89	20.43	0.34	20.76	−2.37	1.25
	NGC 3862	S0	−21.51	20.16	0.98[b]	23.22	−1.53	1.77
	NGC 3873	E	−21.31	20.13	0.72	22.24	−2.03	1.51
	NGC 3886	E	−21.10	20.07	0.41	20.86	−2.36	1.33
	NGC 3910	E	−21.23	20.21	0.64	21.90	−2.10	1.46
	NGC 3937	E	−21.42	20.15	0.91	22.95	−1.89	1.55
	NGC 3940	E	−21.16	20.42	0.72	22.35	−2.02	1.50
A1383	G1	cD	−22.21	19.61	0.79	21.70	−1.67	1.88
A1413	G1	cD	−22.99	19.28	1.20	22.91	−1.72	2.16
Coma	NGC 4816	S0	−21.19	20.82	1.21[b]	24.34	−1.54	1.66
	NGC 4839	cD	−21.43	20.47	1.11	23.72	−1.65	1.71
	NGC 4840	E	−20.33	20.95	0.26	20.96	−2.36	1.19
	NGC 4841	S0	−21.42	20.23	0.92	22.97	−1.75	1.45
	NGC 4864	S0	−20.46	20.69	0.33[b]	21.14	−2.10	1.16
	NGC 4872	E	−21.00	20.55	0.74	22.59	−1.95	1.40
	NGC 4876	E	−19.81	21.32	−0.12	19.24	−3.16	1.07
	NGC 4881	E	−20.53	20.97	0.62	22.56	−2.02	1.29
	NGC 4906	E	−19.88	21.28	0.22	21.09	−2.77	1.01
	NGC 4921	E	−20.46	21.04	0.60	22.54	−1.95	1.25
	NGC 4926	S0	−21.02	20.51	0.68	22.34	−1.98	1.37
	NGC 4927	E	−20.64	20.73	0.52	21.92	−2.21	1.30
	NGC 4952	E	−21.12	20.34	0.64	22.04	−2.09	1.41
	NGC 4957	E	−20.98	20.56	0.77	22.79	−1.92	1.40
	IC 3957	E	−19.56	21.98	0.28	21.96	−2.15	1.18
	IC 3959	E	−20.17	21.26	0.34	21.58	−2.17	1.38
	IC 4051	E	−20.73	20.78	0.66	22.49	−2.13	1.31
	IC 4133	E	−19.75	21.73	0.34	21.99	−2.39	1.11
	IC 832	E	−20.39	21.02	0.49	22.06	−2.18	1.23
	IC 842	E	−19.72	21.71	0.45	22.52	−2.35	1.10
	RB 129	E	−18.66	22.56	0.15	22.02	−2.24	0.87
	RB 195	E	−17.12	24.05	−0.49	19.41	−2.99	0.58
	RB 224	E	−18.68	22.50	−0.22[b]	19.79	−2.67	0.78
	RB 241	E	−20.07	21.36	0.45	22.16	−2.01	1.16
	RB 268	E	−19.77	21.91	0.87	24.36	−1.57	1.24
	RB 31	E	−17.65	23.36	−0.22[b]	20.73	−2.68	0.62
	13 29	E	−19.81	21.57	0.31	21.72	−2.49	1.14
	18	E	−19.13	22.06	0.29[b]	22.20	−2.50	0.95
	19	E	−17.95	23.13	−0.39[b]	19.30	−2.84	0.63
	21	E	−19.02	22.40	−0.51[b]	17.62	−3.14	0.73
	22	E	−17.08	24.06	−0.40[b]	20.12	−2.44	0.53
	23	E	−18.14	22.96	0.27[b]	23.03	−1.91	0.81
	25	E	−17.75	23.30	−0.16[b]	21.02	−2.52	0.69
	29	E	−18.33	22.88	−0.44[b]	18.71	−2.86	0.70
	33	E	−19.59	21.81	0.44	22.62	−1.97	1.10
	37	E	−17.69	23.40	−0.25[b]	20.49	−2.45	0.64
	38	E	−18.19	22.74	0.02[b]	21.54	−2.33	0.72
	40	E	−18.20	23.12	0.18	20.63	−2.49	0.78
	41	E	−18.25	22.93	−0.11	20.91	−2.40	0.80
	48	E	−18.77	22.44	0.11	21.64	−2.21	0.91

TABLE 3—*Continued*

Cluster	Galaxy	type	M_{16kpc}	μ_{2kpc}	log r_e	μ_e	β	log r_H
A1691	G1	D	−22.41	19.83	1.34	23.58	−1.45	1.83
A1767	G1	cD	−22.53	19.64	1.51	24.11	−1.32	1.80
	G2	E	−21.83	19.70	0.60	21.16	−2.12	1.51
A1785	G1	cD:	−21.94	19.84	0.37	22.96	−1.73	1.70
A1795	ZW162010	cD	−22.19	20.00	1.45	24.10	−1.30	2.09
A1809	NGC 5338	cD	−22.48	19.45	1.05	22.45	−1.60	2.01
	G2	E	−21.54	20.18	0.92	22.88	−1.79	1.61
	G3	E	−21.18	20.43	0.46	21.02	−2.08	1.31
A1904	G1	cD	−22.41	19.61	1.31	23.50	−1.49	1.85
A1913	ZW104027	cD	−21.64	19.98	0.95	22.80	−1.74	1.77
	ZW104025	E	−21.40	20.02	0.46	20.79	−2.08	1.32
	ZW104021	E	−21.41	20.32	0.83[b]	22.44	−1.68	1.40
	ZW104022	E	−21.38	20.08	0.52	21.12	−2.03	1.38
	ZW104023	E	−21.31	20.18	0.58	21.46	−1.96	1.47
	G7	E	−21.10	20.50	0.68	22.21	−1.86	1.36
A1983	ZW105054	D	−21.23	20.91	1.33	24.62	−1.32	1.76
	ZW105053	E	−21.49	20.16	0.69	21.84	−1.83	1.55
	ZW105055	E	−20.96	20.82	0.91	23.28	−1.59	1.35
	G6	E	−21.32	20.30	0.81	22.62	−2.03	1.48
	G7	E	−21.10	20.35	0.44	20.99	−2.62	1.27
	G8	E	−21.00	20.61	0.61	21.92	−2.25	1.40
A1991	G1	D	−22.06	20.19	1.47	24.31	−1.26	1.84
A2028	G1	cD	−22.33	19.70	1.37	23.83	−1.47	1.96
A2029	IC 1101	D	−23.05	19.49	1.66	24.16	−1.49	2.11
A2052	UGC 9799	D	−22.26	20.08	1.56	24.50	−1.50	1.84
A2061	ZW165041	cD	−22.47	19.43	1.09	22.58	−1.66	1.87
	G2	E	−22.03	19.76	0.89	22.21	−1.95	1.63
	G3	gE	−22.09	19.75	0.97	22.51	−1.76	1.80
A2063	G1	D	−21.67	20.46	1.37	24.24	−1.08	1.57
	G2	E	−20.57	20.91	0.41	21.47	−1.53	1.22
	G3	E	−20.10	21.14	0.29[b]	21.11	−1.96	1.08
A2065	G1	D	−22.25	20.14	1.64	24.89	−1.44	2.06
	G2	gE	−22.20	20.05	1.28	23.73	−1.67	2.01
A2089	G1	gE	−23.01	18.86	1.13[b]	22.28	−1.70	1.86
A2107	UGC 9958	D	−22.39	19.68	1.32	23.59	−1.65	1.86
A2124	UGC 10012	D	−22.57	19.74	1.47	24.02	−1.53	1.76
A2142	G1	cD	−22.86	19.45	1.60	24.02	−1.33	2.08
	G2	D	−22.68	19.76	1.55	24.09	−1.23	1.94
A2147	UGC 10143	cD	−22.05	19.87	1.17	23.34	−1.49	2.14
Hercules	NGC 6041	gE	−22.42	19.53	1.20	23.11	−1.76	1.96
	NGC 6034	cD	−21.86	19.76	1.27	24.11	−1.70	1.90
	NGC 6042	gE	−21.55	20.32	1.13	23.66	−1.79	1.90
	NGC 6044	E	−21.37	19.91	0.20	19.30	−2.73	1.33
	NGC 6047	E	−21.81	19.86	1.00	22.96	−1.85	1.58
	NGC 6055	E	−21.70	19.93	0.95	22.88	−1.93	1.63
	NGC 6057	E	−21.00	20.40	0.44	21.11	−2.26	1.37
	NGC 6061	E	−21.90	19.71	0.83	22.12	−2.07	1.58
	IC 1184	E	−21.08	20.51	0.59	21.72	−2.36	1.50
	IC 1185	E	−21.23	20.28	0.64	21.85	−2.30	1.54
A2152	UGC 10187	E	−21.40	19.78	0.60	21.61	−2.10	1.45
	G2	E	−21.10	20.44	0.83	22.99	−1.94	1.42
	G3	E	−21.19	20.21	0.72	22.38	−1.99	1.33
A2162	NGC 6086	cD	−21.81	20.02	0.92[b]	22.54	−1.58	1.96
	G2	E	−20.25	21.22	0.68	23.15	−1.79	1.33
	G3	E	−19.84	21.59	0.30	23.35	−2.03	1.13
A2184	G1	E	−21.20	20.44	0.71	22.17	−1.84	1.50
A2197	NGC 6173	D	−22.69	19.47	1.37	23.39	−1.59	2.13
	NGC 6146	gE	−22.39	19.67	1.01	22.25	−2.04	1.75
	NGC 6160	D	−22.47	19.59	1.34	23.54	−1.40	1.80
A2199	NGC 6166	cD	−22.28	19.67	1.18	23.08	−1.81	2.07
A2249	ZW198012	D	−22.14	19.91	1.19	23.33	−1.64	1.79
	G2	E	−21.86	19.89	0.90	22.41	−1.90	1.60
	G3	E	−21.96	19.72	0.81	21.96	−1.89	1.63
A2255	G1	D	−22.44	19.78	1.46	23.97	−1.39	1.87
	G2	D	−22.25	19.82	1.33[b]	23.83	−1.42	1.90
	G3	E	−22.16	19.80	1.16	23.16	−1.59	1.74
A2256	ZW355027	D	−22.35	19.82	1.33	23.52	−1.52	1.86
	UGC 10726	E	−22.21	19.60	0.93	22.10	−1.72	1.63
	G4	E	−21.59	20.01	0.68	21.68	−1.88	1.41
A2271	ZW355030	D	−22.31	20.00	1.53	24.25	−1.32	1.69
A2366	G1	cD	−22.27	19.49	0.87	22.09	−1.62	1.87
A2400	G1	D	−22.18	19.98	1.16	23.18	−1.65	1.72
	G2	E	−22.08	19.78	0.94	22.42	−1.76	1.59
A2420	G1	cD	−22.30	20.05	1.45	24.04	−1.42	1.91
	G2	E	−21.31	20.44	0.75	22.35	−1.84	1.33

TABLE 3—*Continued*

Cluster	Galaxy	type	M_{16kpc}	μ_{2kpc}	log r_e	μ_e	β	log r_H
A2440	G1	E	−21.17	20.69	1.00	23.46	−1.58	1.45
	G2	E	−21.01	20.96	1.13	24.16	−1.44	1.60
	G3	E	−20.71	20.84	0.56	22.01	−1.92	1.36
A2457	G1	D	−22.07	19.91	1.15	23.13	−1.62	1.77
A2469	G1	E	−21.45	20.36	0.84	22.50	−1.82	1.47
A2572	NGC 7597	cD	−21.90	20.01	1.23	23.62	−1.48	1.64
	NGC 7602	E	−21.43	20.14	0.48	20.95	−1.82	1.36
A2589	NGC 7647	cD	−22.05	20.09	1.46	24.18	−1.32	1.89
A2593	NGC 7649	D/S0:	−22.08	20.17	1.41	24.09	−1.18	1.70
	IC 1487	E	−21.74	20.02	0.84	22.21	−1.69	1.49
	G3	E	−21.15	20.41	0.60	21.74	−1.92	1.43
	G4	E	−20.76	20.69	0.47	21.45	−2.07	1.29
A2634	NGC 7728	cD	−22.07	19.53	0.79	21.73	−2.14	1.73
	NGC 7720	D	−22.03	19.87	1.17	23.25	−1.50	1.87
	UGC 12733	E	−21.61	19.84	0.73	22.02	−2.11	1.51
	UGC 12744	E	−21.80	19.89	0.96	22.77	−1.91	1.62
A2666	NGC 7768	cD	−22.38	19.32	1.08	22.67	−1.92	1.81
A2670	G1	cD	−22.44	19.57	1.23	23.30	−1.69	2.13
A2700	G1	D	−22.55	20.01	1.62[b]	24.52	−1.29	1.84
Virgo	NGC 4476	E	−21.66	19.91	0.99	22.99	−1.88	1.65
	M87	E	−21.37	20.18	0.72	22.09	−2.01	1.57
	NGC 4406	E	−21.51	20.35	1.21[b]	23.97	−1.66	1.52
	NGC 4459	E	−20.36	21.07	0.44	21.80	−2.46	1.20
	NGC 4552	E	−20.96	20.61	0.88	23.25	−1.75	1.55
CA0340−538	G1	gE	−22.35	19.76	1.29	23.57	−1.77	1.80
	G5	E	−21.85	20.10	0.88	22.40	−2.05	1.68
DC0107−46	IC 1633	gE	−22.79	19.27	1.39	23.33	−1.70	1.91
	G2	E	−21.90	19.92	1.03	22.93	−1.91	1.68
SC1325−31	G1	cD	−22.93	19.32	1.73	24.47	−1.51	2.48
	G2	E	−22.14	19.76	0.89	22.15	−2.13	1.56
	G3	E	−21.99	19.58	0.84	22.08	−2.03	1.63
	G4	E	−21.82	19.78	0.79	22.05	−2.08	1.55
	G5	E	−21.73	19.90	1.02	23.15	−1.84	1.65
	G6	E	−21.66	20.11	1.14	23.73	−1.75	1.69
	G7	E	−21.61	19.86	0.81	22.31	−2.06	1.50
	G8	E	−21.48	19.96	0.56	21.29	−2.35	1.40
	G9	E	−21.39	20.07	0.65	21.81	−2.30	1.38
	G10	E	−21.30	20.21	0.75	22.47	−1.99	1.45
	G11	E	−21.04	20.39	0.34	20.49	−2.56	1.34
SC1328−32	G1	gE	−22.09	20.05	1.30	23.82	−1.71	1.77
	G2	gE	−22.01	20.05	1.17	23.41	−1.81	1.78
	G3	E	−21.54	19.54	0.41	20.50	−2.28	1.37
	G4	E	−20.89	20.25	0.02	19.09	−2.79	1.17
	G5	E	−20.85	20.42	0.21	20.23	−2.38	1.30
	G6	E	−20.27	20.84	−0.08	18.88	−3.88	0.82
	G7	E	−20.25	20.78	−0.04	19.10	−3.48	0.95
SC1331−31	G1	cD	−22.46	19.57	1.72	24.94	−1.43	2.06
	G2	E	−22.15	19.84	0.97	22.40	−1.98	1.66
Centaurus	NGC 4696	gE	−22.09	19.85	1.26	23.52	−1.74	1.76
	NGC 4709	E	−21.27	20.34	1.03	23.47	−1.78	1.69
Fornax	NGC 1399	D[c]	−21.87	19.89	1.40	24.26	−1.47	2.17
	NGC 1336	E	−19.75	21.38	0.31	21.62	−2.52	1.10
	NGC 1351	E	−19.89	21.43	0.46	22.37	−2.26	1.15
	NGC 1374	E	−20.12	21.08	0.28	21.15	−2.42	1.11
	NGC 1379	E	−20.15	20.98	0.16[b]	20.42	−2.87	1.05
	NGC 1387	E	−20.22	21.05	0.50	22.00	−2.66	1.08
	NGC 1389	E	−19.56	21.71	0.06[b]	20.65	−2.68	1.12
	NGC 1427	E	−20.30	20.97	0.47	21.93	−2.26	1.22
AWM 1	NGC 2804	E	−21.94	19.71	0.94	22.56	−1.88	1.67
AWM 2		E	−21.53	20.24	0.94[b]	22.99	−1.72	1.51
AWM 3		E	−21.20	20.53	0.82	22.85	−1.84	1.64
AWM 4	NGC 6051	gE	−22.32	19.60	1.15	23.02	−1.78	1.78
AWM 5	NGC 6269	gE	−22.68	19.04	1.18[b]	22.72	−1.73	1.90
AWM 6		D	−22.41	19.52	1.24	23.24	−1.66	1.80
AWM 7	NGC 1129	D/cD:	−22.95	19.31	1.47[b]	23.48	−1.63	2.00
MKW 1s	0917.5+0115	E	−21.37	20.13	0.80	22.45	−2.01	1.58
MKW 2	1027.6−0255	gE	−22.11	19.50	1.09	22.96	−1.76	1.73
MKW 4	NGC 4073	gE	−22.15	19.74	1.11	22.88	−1.89	1.72
MKW 5	NGC 5400	E	−21.50	20.15	0.87	22.64	−1.94	1.51
MKW 9	1530.0+0451	gE	−21.83	20.21	1.27	23.99	−1.65	1.71
Isolated E's	NGC 1426	E	−18.98	22.29	0.27	22.28	−2.51	1.00
	NGC 1521	E	−21.21	20.31	0.89	22.98	−1.94	1.54
	NGC 4104	gE	−22.32	19.65	0.89	22.89	−1.87	1.76
	NGC 5251	E	−21.71	19.86	0.65	21.46	−2.42	1.39
	NGC 6721	E	−21.22	20.08	0.66	21.91	−2.17	1.38
	NGC 6758	E	−20.79	20.60	0.82	23.05	−1.97	1.46

TABLE 3—*Continued*

Cluster	Galaxy	type	M_{16kpc}	μ_{2kpc}	log r_e	μ_e	β	log r_H
Isolated E's	NGC 6854	E	−21.69	19.62	0.81	22.23	−1.99	1.53
	NGC 7014	E	−20.76	20.66	0.99	23.85	−1.72	1.54
	NGC 7168	E	−20.11	21.12	0.31	21.32	−2.54	1.15
	IC 4307	E	−21.33	20.01	0.50	21.22	−2.20	1.36
	IC 4314	E	−21.32	20.14	0.61	21.77	−2.04	1.48
	IC 5328	E	−21.33	20.15	0.48	20.69	−2.49	1.47
	0815.6+6708	E	−20.49	20.85	0.46	21.82	−2.14	1.25
	0817.2+6641	E	−21.42	19.92	0.60	21.60	−2.06	1.48
	0824.8+6330	S0	−21.28	20.02	0.56	21.49	−2.16	1.37
	0838.6+6438	E	−20.90	20.56	0.72	22.72	−1.92	1.39
	0839.5+6509	E	−20.61	20.79	0.38	21.35	−2.23	1.39
	0841.7+6418	E	−21.29	20.15	0.66	22.01	−2.08	1.47
	1205.5+2531	E	−21.27	20.15	0.81	22.66	−1.86	1.52
	1208.0+2542	E	−20.73	20.55	0.38	21.14	−2.27	1.26
	1213.1+2717	E	−20.29	21.00	0.34	21.41	−2.24	1.27
	1338.4+2629	E	−21.94	19.99	0.50	20.47	−2.58	1.36
	1339.5+2638	gE	−22.54	19.57	1.34	23.58	−1.66	1.88
	1341.4+2539	E	−20.72	20.69	0.46	21.64	−2.09	1.26

[a] Possible extended envelope; uncertain owing to limits of CCD field size.
[b] Poor $r^{1/4}$ fit.
[c] Dumbbell system in common envelope.
[d] Extremely small envelope, possible D system.
[e] Uncertain cD envelope owing to size of object and limits of plate material.

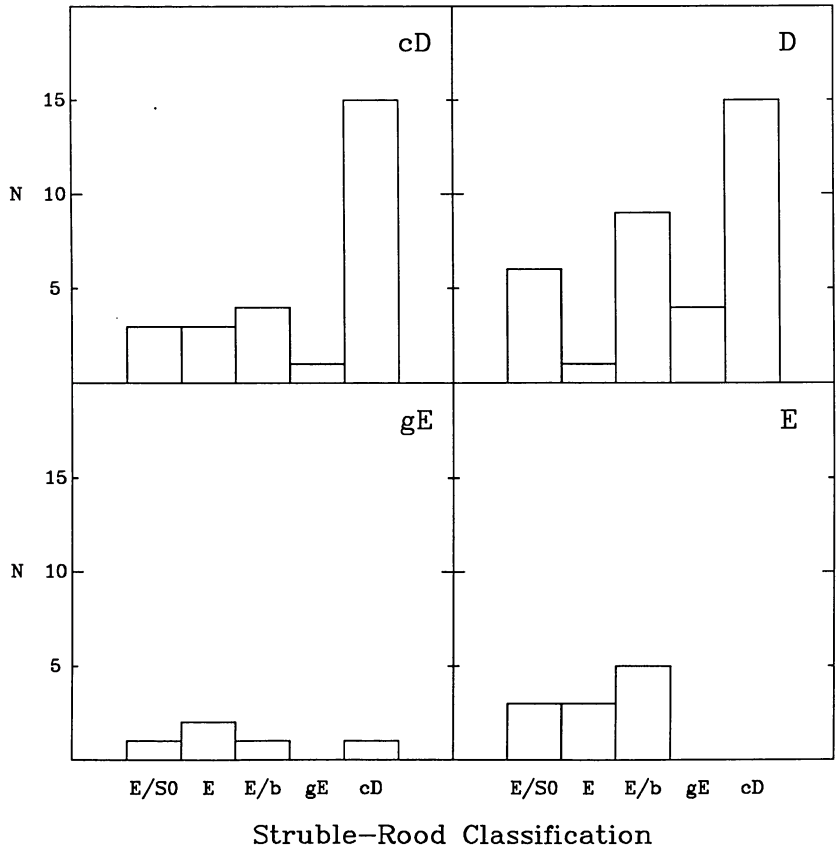

FIG. 3.—Visual classification from Sky Survey prints (Struble and Rood 1986) versus profile classification. Each of the four morphological classes is discussed in the text. Note that visual classification as cD type is more closely related to profile slope than to the real presence of extended envelopes (Malumuth 1983).

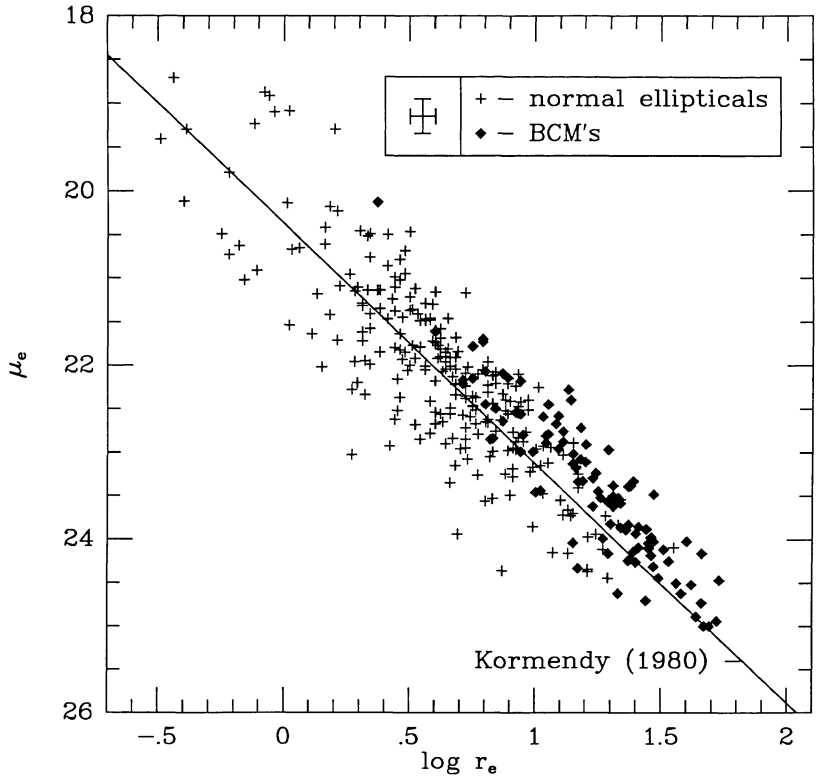

FIG. 4.—Effective surface brightness (μ_e) versus effective radius (r_e) from $r^{1/4}$ fits. The relation for normal ellipticals from Kormendy (1980) is also shown. Enlarged radii for BCMs are evident from the fact that 87% of these objects lie to the right of the relation, whereas the normal ellipticals scatter evenly. A typical error bar is displayed at the top.

the observations from Paper I combined with the results from Malumuth (1983) begin to define a very clear trend of structural parameters which distinguish BCMs from other bright ellipticals of similar luminosities.

The first difference is that BCMs have enlarged characteristic radii when compared with ellipticals of similar luminosity (see Fig. 6, Paper I). This is displayed in Figure 4, where over 87% of the BCMs lie above the relation of Kormendy (1980), yet the normal ellipticals are scattered evenly around this line. A Kolmogorov-Smirnov (K-S) test rejects at the 99.9% level the null hypothesis that the two sets are drawn from the same population. Since lines of constant luminosity have a slope of -5 in this diagram, this deviation is an effect neither of extreme luminosities nor of the large changes in effective surface brightness. BCMs are simply more diffuse and enlarged with respect to the average structure of non–first-ranked ellipticals.

A second difference is that BCMs have shallower profiles than normal ellipticals. This is shown in Figure 5, a histogram of profile slope β (see also Fig. 3.11 of Malumuth 1983) for BCMs and normal ellipticals. Notice that the BCM distribution peaks to the right of the normal ellipticals, with a mean of $\beta = -1.6$ compared with a mean for normal ellipticals of $\beta = -2.1$. A K-S test rejects the null hypothesis that the two sets are drawn from the same population at the 99.9% level. This agrees with the result of Thuan and Romanishin (1981), who found that BCMs in poor clusters were more diffuse than normal ellipticals. In this study, the term "diffuse" is meant to signal the enlarged radii and shallow profile slope producing a large extended galaxy to the eye. There is no distinction between D- and cD-type profiles with respect to profile slope. There is also no apparent correlation between the presence of companions and shallow profiles.

It should be noted that the deviations of BCM structure from that of normal ellipticals is not a luminosity effect of the type used to explain variations in normal elliptical structure as proposed by Djorgovski (1985), since there exists some overlap between the brightest isolated and cluster ellipticals and the BCMs. This can be most easily seen in Figure 6, a plot of log r_{22} versus log r_{24}, the radius of a galaxy at the 22 and 24 mag arcsec^{-2} isophote, respectively. Although the brightest BCMs are outside the range of the normal ellipticals, the separation of the diagram into two distinct families is clear. Shallow profiles can also explain the small dispersion in luminosity for BCMs. There is very little change in central surface brightness for the bright end of the luminosity function and a standard profile, combined with the relatively small change in profile slope, produces an aperture magnitude which varies only a small amount from cluster to cluster.

Historically, BCMs have always been considered to be objects with low central surface brightnesses, despite the profiles published by Oemler (1976), which show high inner surface brightness for most cD galaxies. This study finds the same trend of *high* inner surface brightnesses for BCMs and

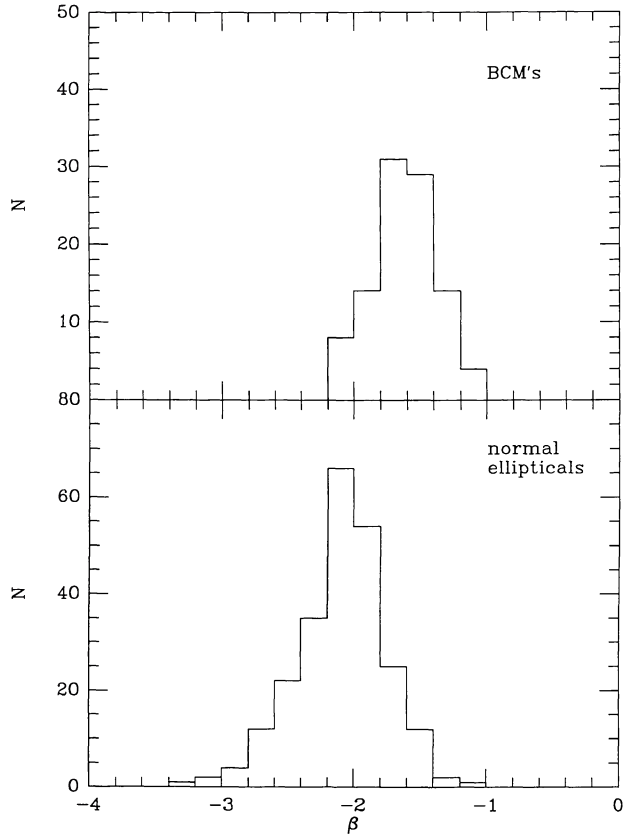

FIG. 5.—Histograms of profile slope (β) for BCMs and normal ellipticals. The distribution of profile slopes for BCMs is noticeably shallower than for the normal ellipticals (see also Fig. 3.11 of Malumuth 1983).

is displayed in Figure 7 as a plot of magnitude ($M_{16\ \mathrm{kpc}}$) versus surface brightness at the 2 kpc radius ($\mu_{2\ \mathrm{kpc}}$). In fact, the trend of increasing inner surface brightness with magnitude appears smooth and unbroken, unlike the magnitude-radius relation from Paper I or the radius-radius relation in Figure 6. Some individual objects, such as NGC 6166 in A2199 and A85-G1, do have unusually low inner surface brightnesses, but these objects are rare and should be considered peculiar in nature. In fact, both systems display emission features in their spectra (Bertola *et al.* 1986; Schombert and Tonry 1987) perhaps the remnant of a very recent merger of a gas-rich system, and the lower central surface brightness may be a temporary effect before relaxation into a more centrally concentrated core. On the other hand, owing to the diffuse nature of BCMs, the average surface brightness at the effective radius ($\langle\mu\rangle$), will be much lower than that of normal ellipticals (see Fig. 11 of Schombert 1984). This is an effect of shallow profiles and large effective radii, which combine to produce artificially low values of $\langle\mu\rangle$. The important point to note is that the central concentration, as determined from the profiles, is as great as , or greater than other normal ellipticals of similar luminosity.

Overall, BCMs have the same general appearance as normal ellipticals, but differ as a group in enlarged structure. This would not be expected from extrapolation of normal elliptical structure to higher luminosities as seen in Figure 6, and the other characteristics of BCMs indicate the influence of a special process on their formation.

d) *Mergers*

A complication arises when BCMs are compared with other bright cluster ellipticals in a search for merger effects in their

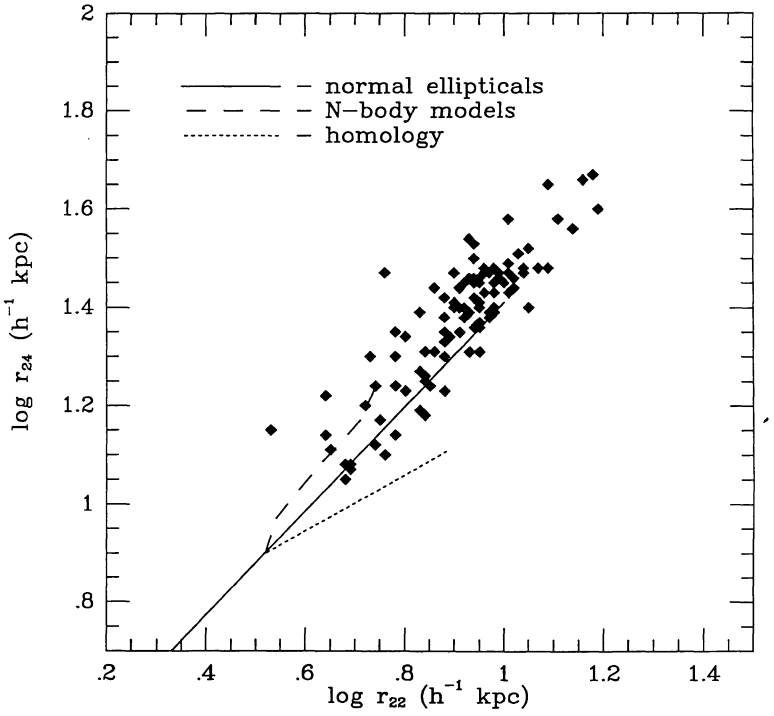

FIG. 6.—Isophotal radius at 24 mag arcsec^{-2} (r_{24}) versus isophotal radius at 22 mag arcsec^{-2} (r_{22}). These radii were chosen to be above the level of cD envelopes and reflect only the inner structure of BCMs. The predictions of homology merger calculations and *N*-body merger models (Duncan, Farouki, and Shapiro 1983; Farouki, Shapiro, and Duncan 1983) for 16 L_* growth from a 1 L_* progenitor are also shown.

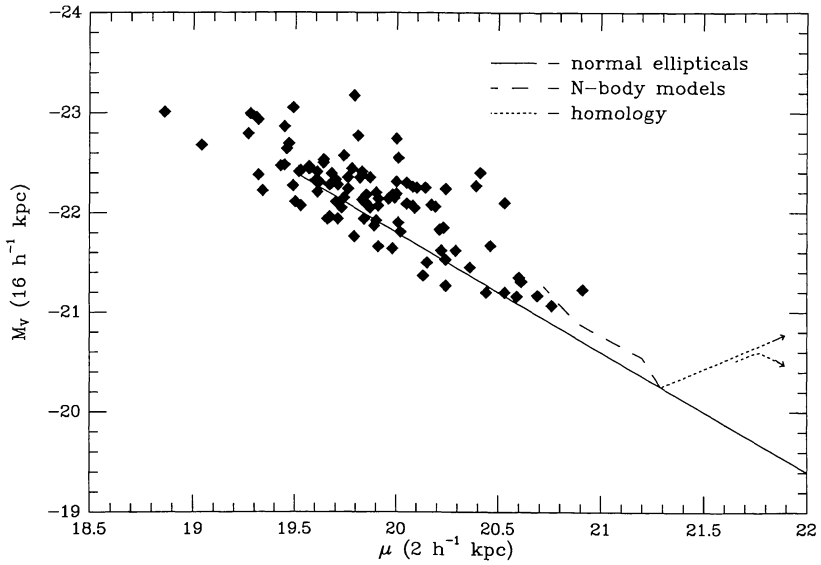

FIG. 7.—Integrated magnitude ($M_{16\ \mathrm{kpc}}$) vs. inner surface brightness ($\mu_{2\ \mathrm{kpc}}$). Contrary to the popular misconception of low central surface brightness for D and cD galaxies as predicted by homology models, the BCMs of this sample have inner surface brightnesses as high as or higher than those of the normal ellipticals. As in Fig. 6, the predictions of homology and *N*-body models are shown.

structure. This is the problem of assuming that the second-ranked or third-ranked galaxies are free from mergers themselves. This would seem unlikely in light of the models by Malumuth and Richstone (1984) and Merritt (1984), where mergers are found to be an ongoing process among all bright ellipticals in the cores of rich clusters. Comparisons with isolated bright ellipticals may not escape this problem because of indications of at least one accretion (Quinn 1984) based on estimates of high fractions of shell ellipticals in the field (Malin and Carter 1983), and the possibility of runaway mergers forming apparently isolated galaxies (Carnevali, Cavaliere, and Santangelo 1981). What will be assumed in the following discussion is that if BCMs are merger products, then they have at least undergone a more extreme history of mergers than their lesser companions.

In previous papers merger observations have been compared with the standard cannibalism models (Hausman and Ostriker 1978) because of the simple power of their predictions and ease of calculation. The basic premise in these models is the assumption of homology, or the conservation of energy and scale before, during, and after a merger. However, the conservation-of-energy assumptions could easily be violated if the process of merging is violent or if infalling galaxies maintain their identities to the core (White 1982). Despite the possible difficulties, homologous mergers have enjoyed a good deal of confirmation in observations. The relationship between mean structure parameters and absolute magnitude from Hoessel, Gunn, and Thuan (1980) is in good agreement with the predictions of hierarchical mergers and rules out the accretion scenario. Thomsen and Frandsen (1983) interpret the (μ_e, log r_e)-diagram in terms of homologous mergers and conclude that dynamical evolution predicts the same slope as their data. Malumuth (1983) also uses homology results to confirm evidence of dynamical growth.

As a check on the homology predictions, the data in this paper are also compared with the predictions from *N*-body simulations by Duncan, Farouki, and Shapiro (1983, hereafter DFS) and Farouki, Shapiro, and Duncan (1983, hereafter FSD). This set of papers models both hierarchical and accretion scenarios of mergers for up to 16 L_* of growth. Each of these papers derives density profiles (cf. Fig. 5 of DFS, Fig. 3 of FSD) for each stage of merging, which have been used below in comparison with observations. The original progenitor models in their studies were scaled to match the properties of an L_* galaxy in Figure 1. The later stage profiles were then rescaled and reduced in the same manner as the data.

Both homology and *N*-body results predict luminosity growth with each merger. However, homology predicts a decrease in central surface brightness, while the *N*-body simulations show an increase in the central concentration. This increase is apparently the result of two processes, one the effect of relaxation on the remnant and the other a survival of the inner cores of accreting companions, not totally disrupted during infall, adding their high densities to the core. Figure 7 displays the different predictions and the data in a plot of magnitude $M_{16\ \mathrm{kpc}}$ versus $\mu_{2\ \mathrm{kpc}}$. Since $M_{16\ \mathrm{kpc}}$ is determined by integrating surface brightness profiles, it has the advantage of being free of contamination by multiple nuclei. Both models, homology and *N*-body, are assumed to start with an L_* progenitor and evolve as shown either by Figure 1 in Ostriker and Hausman (1977), Figure 3 of FSD, or Figure 5 of DFS. Homology predicts increasing magnitude and decreasing surface brightness until the aperture size equals the effective radius; then a decrease in magnitude is expected. This is in direct contradiction to the observations for BCMs; however, the predictions of the *N*-body simulations give roughly the same relation as seen by BCMs.

The homology and *N*-body models both predict radial growth in size with each merger, but since homology uses scaling arguments, this growth is linear. The *N*-body results present a scenario where the galaxy is disrupted during infall and more matter is placed in the outer regions. This does not

form cD envelopes, as hoped by the authors, because of the large scale lengths associated with these envelopes. But their models do produce shallow profiles of slopes similar to those of D and cD galaxies. Both predictions are displayed in Figure 6, and again the *N*-body models predict the placement of the BCM data.

If mergers are to be imposed as an explanation of BCM structure, then the scenarios outlined by FSD and DFS are more in line with observations than the predictions of homology scenarios. To form D and cD galaxies, the above comparisons indicate 16–20 L_* growth for 1–5 L_* progenitors. The exact process of merging is not known; however, there is every reason to believe that the bright galaxies in clusters would be the most likely candidates, and the observed D and cD galaxy luminosities are not outside the range of growth.

Another interesting result from examination of the *N*-body merger remnant profiles is that they are to a large extent $r^{1/4}$ in shape. This is not a surprising result, since the simulations of Villumsen (1982) and May and van Albada (1984) also produce merger remnants which are $r^{1/4}$ in shape. This general trend in the profiles from theoretical studies has led many of the above authors to conclude that the $r^{1/4}$ law is a natural density relation that follows from a system which is disrupted and then is allowed to relax. The observations of this paper support this hypothesis, since the dominance of the $r^{1/4}$ relation at the bright end of the sample is quite prominent. The above statement may overgeneralize the evidence of mergers, since several other detailed CCD surface photometry studies (Lauer 1986; Djorgovski 1985) argue against any smooth relation to describe the structure of ellipticals. The disclaimer should be made that ellipticals are certainly *not* $r^{1/4}$ over a full range of surface brightness, and the similarity between the computer simulation profiles and the data may be an effect of forcing a particular fitting function on the profiles. However, qualitatively, the $r^{1/4}$ relation is a reasonable describer of the interiors of both BCMs and the merger simulations.

An extreme opinion about all bright ellipticals can be made if we assume that the *only* method of producing $r^{1/4}$ profiles is by mergers. In this case, all ellipticals brighter than $M_V = -21$ are merger products. A diagram suggestive of this interpretation can be found in Figure 8, where $M_{32\,\mathrm{kpc}}$ is plotted against log r_e from $r^{1/4}$ fits. The 32 kpc aperture size was selected so as to include as much light as possible for BCMs, while lying well inside the extended envelopes of cD galaxies, which are assumed to form by a process not directly related to mergers. In this diagram there is the suggestion of a break in the trend of brighter galaxies, with larger values of r_e around the $M_V = -21$ point. This break is also at the same point found by Davies *et al.* (1983), where the kinematics of ellipticals change from rotators for the faint ellipticals to being supported by anisotropic velocity distributions. The break was also suggested by the different (L, r)-relations found by Kormendy (1977) and Strom and Strom (1979). Kormendy's sample was concerned with bright ellipticals and hence found a shallower relation than the seven-cluster sample of Strom and Strom, which measured a large number of faint ellipticals. An analysis of bright ellipticals by Romanishin (1986) also found a relation similar to Kormendy's; therefore, the

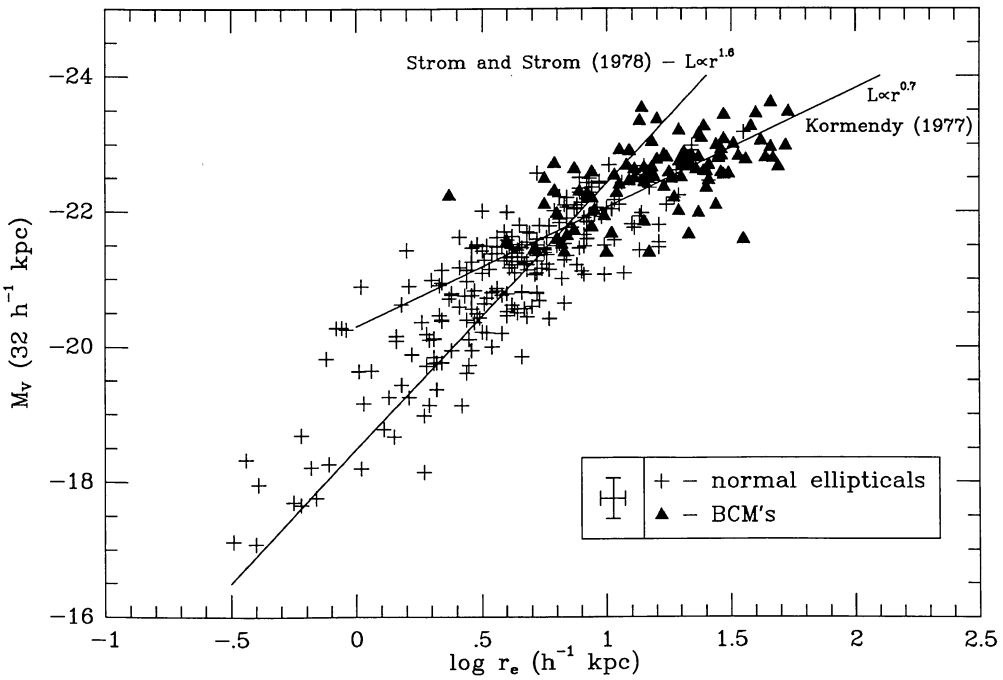

FIG. 8.—Magnitude ($M_{32\,\mathrm{kpc}}$) vs. radius (r_e) diagram. The two relations from Strom and Strom (1979) (dominated by faint ellipticals) and Kormendy (1977) (dominated by bright ellipticals) are also shown. The BCMs are expected to deviate from the relation as a result of their enlarged radii. However, the bright isolated ellipticals also follow the Kormendy relation above $M_V = -21.5$. This break is near the same magnitude where Davies *et al.* (1983) determined that the internal kinematics of ellipticals changes from rotational support to anisotropic velocity support.

different relations for faint and bright ellipticals are not an effect of two different authors and procedures. It should be noted that the isolated ellipticals of this sample are also $r^{1/4}$, and any merger explanation for their shape must assume a runaway merger scenario as proposed by Carnevali, Cavaliere, and Santangelo (1981) in order to reduce the original cluster to one member. Mergers of bright ellipticals may also be primordial, that is, mergers of large protogalactic clouds in order to form anisotropic distributions, rather than mergers between systems in a recent epoch. At the very least, the break in Figure 8 reflects the change in the kinematics of bright ellipticals in their structure.

e) *Cluster Properties*

If mergers are responsible for BCMs, then it has been shown by several authors (Malumuth and Richstone 1984; see references therein) that this growth will be at the expense of fainter members. The galaxy with the highest probability of being accreted will be near slow-moving ellipticals, which, given some mass segregation in clusters, should be among the higher ranked galaxies. Hence, as the luminosity of the first-ranked member grows, the luminosity of the second- and third-ranked members should decrease (actually it is the ranking that changes, since the second- and third-rank members are consumed). This hypothesis can be tested by plotting the luminosity of the BCM against the difference in the luminosities of the BCM and the second-ranked galaxy, shown in the top panel of Figure 9. M_1 is the total integrated magnitude of the galaxy excluding the luminosity from cD envelopes (assumed not to be related to merger effects; see subtraction method in Paper III). The trend of increasing BCM luminosity with increasing difference between the BCM and the second-ranked member is presented as evidence for dynamical evolution in this sample. There is a well-known selection effect of picking the brightest member of any sample for comparisons in ranking (Malumuth and Richstone 1984);

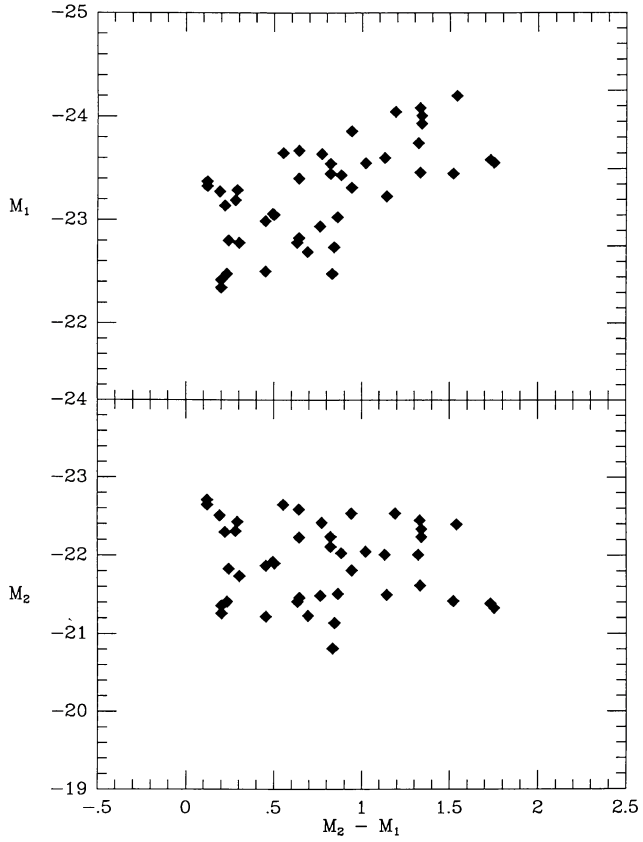

FIG. 9.—Magnitudes of the first- and second-rank galaxies (M_1, M_2) in each cluster versus the difference in their magnitudes ($M_2 - M_1$). Dynamical evolution would imply that the luminosity of the BCMs increases at the expense of lesser cluster members, as seen with the positive correlation in the top panel. This correlation is not a selection effect, since there is no corresponding anticorrelation in the M_2 vs. $M_2 - M_1$ diagram of the bottom panel. These plots compare favorably with the cluster evolution simulations of Malumuth and Richstone (1984) (see their Fig. 7).

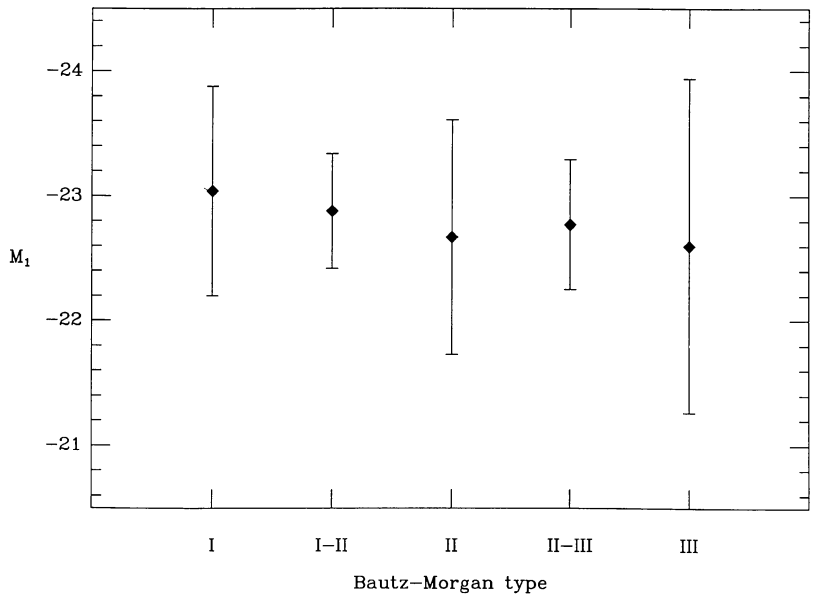

FIG. 10.— M_1 vs. Bautz-Morgan cluster type. Error bars represent 2 σ dispersions from the mean.

however, a test of the severity of this effect is to plot the luminosity of the second-ranked member against the difference in the luminosities of the BCM and the second-ranked galaxy in search of an anticorrelation. This plot is found in the bottom panel of Figure 9, and there is no evidence of such an anticorrelation. A comparison between Figure 9 and Figure 7 of Malumuth and Richstone (1984) reveals a good correspondence between their cluster simulations and the data.

There is a weak correlation of Bautz-Morgan class taken from Leir and van den Bergh (1977) and BCM luminosity (Fig. 10). Bautz-Morgan class is assumed to be some visual measure of the dynamical state of a cluster, and the increase in BCM luminosity with more evolved cluster state would argue for growth by mergers. The large scatter for the Bautz-Morgan type III clusters probably reflects the multiple subcluster nature of these systems. There is also a weak correlation between the BCM corrected luminosity and cluster richness (as given by Abell counts from Struble and Rood 1986 and Bahcall 1980) displayed in Figure 11. The hypothesis here is that richer clusters provide more candidates for accretion and, therefore, brighter BCMs (see also Fig. 3 of Schneider, Gunn, and Hoessel 1983). Figure 12 displays BCM corrected luminosity and cluster velocity dispersion. Again, a weak

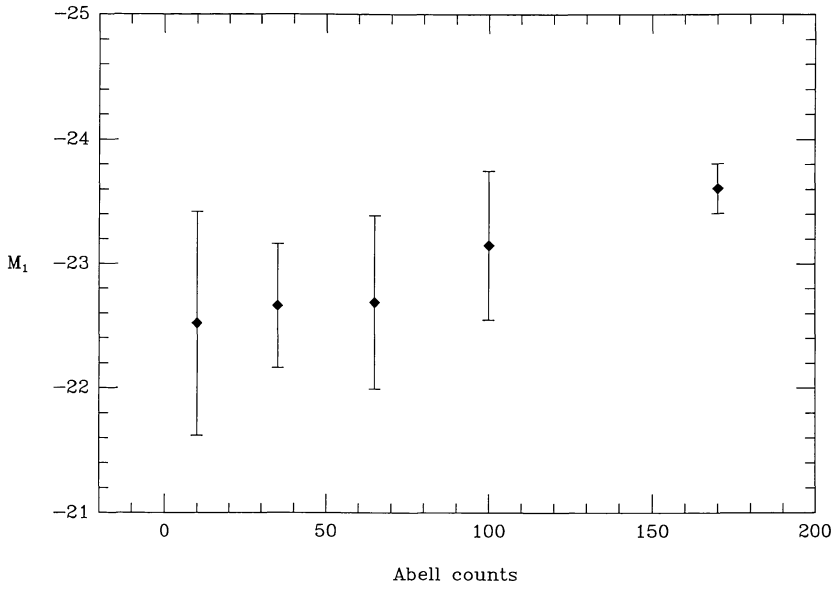

FIG. 11.— M_1 vs. cluster richness (Abell counts). The increase in BCM luminosity with cluster richness (as determined from Abell counts given by Struble and Rood 1986 and Bahcall 1980, binned in 0–19, 20–49, 50–79, 80–120, and >120 groups) is weakly support by the above plot. The error bars are 2 σ dispersions on the means.

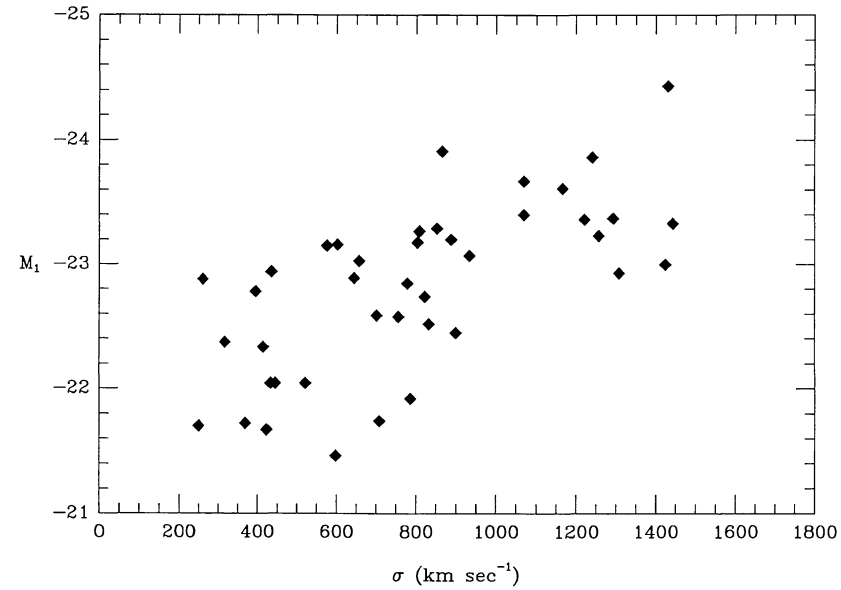

FIG. 12.— M_1 vs. cluster velocity dispersion. There is a slight tendency for the luminosity of the BCM to increase with cluster velocity dispersion; see discussion in text.

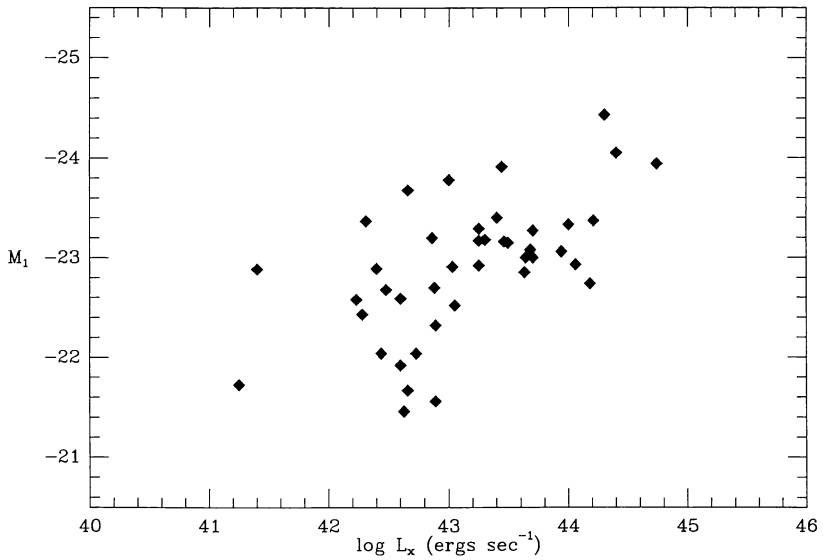

FIG. 13.— M_1 vs. total cluster X-ray luminosity. Another weak correlation with a global parameter that measures the dynamic state of the cluster argues that the dynamical growth of BCMs must have been an early process as proposed by Merritt (1984); see discussion in text.

correlation (coefficient = 0.67) is present, with brighter BCMs occupying clusters with high velocity dispersions. The underlying physics is not clear in this situation. It is expected from a simple theory of cannibalism that a cluster with a lower velocity dispersion would have a higher rate of mergers and, hence, a brighter BCM. The average velocity dispersion of the bound population to a BCM is expected to be similar to the internal velocity dispersion of the galaxy, on the order of 200–300 km s^{-1} (Cowie and Hu 1986). On the other hand, it has been argued by Tonry (1985) that the low-velocity members are missing in evolved clusters because they have already merged with the central members. With this low-velocity population disappearing, the average cluster velocity dispersion would increase. It is this second scenario that is supported by Figure 12. Figure 13 displays BCM luminosity versus cluster X-ray luminosity from Valentijn and Bijleveld (1983). Although there is a slight tendency for brighter BCMs to be associated with X-ray–luminous clusters, this correlation (coefficient = 0.60) is by no means strong and could be a selection effect of cluster richness in the sample. X-ray luminosity is considered to be a measure of the dynamical age of a cluster (Forman and Jones 1982), and the plot here is as suggestive as Figures 10, 11, and 12.

The lack of a strong cluster property correlation with luminosity of BCMs argues that most of the evolution of these objects was a local phenomenon. Given the occurrence of at least one cD not in the cluster core, but in a local subcluster (NGC 6034 in Hercules), the most likely scenario is the one proposed by Merritt (1984), where strong evolution occurs in early subclumps before cluster virialization. Early mergers would explain these weak correlations, which are reflecting some effect of early universe density enhancement and not the overall state of the cluster at the current epoch. Yet early evolution would preserve the ranking effect (M_1 vs. $M_2 - M_1$) after the subclusters collapse to form a single cluster identity. This scenario would also explain the absence of a bound population of accreting galaxies, but it remains unclear whether BCMs are still undergoing mergers with the multinucleus companions.

IV. CONCLUSIONS

The main purpose of this paper is to support the idea that BCMs have particular structural deviations, as seen in surface photometry profiles, which are best explained by comparisons with merger simulations. These special properties are enlarged characteristic radii, shallow profile slopes, and high inner surface brightnesses. From the appearance of the profiles, it is possible to outline the morphological types gE, D, and cD ellipticals: gE galaxies are typified by their large size, D galaxies are a gE type with a very shallow slope ($\beta < -1.7$) and cD galaxies are a D type with a large, faint extended envelope.

Comparison with the predictions of homology calculations (Hausman and Ostriker 1978) and N-body merger simulations (DFS; FSD) rules out the homology scenarios, but is in strong agreement with the remnant profiles from the N-body work. This is presented as the strongest argument that BCMs owe their properties and extreme luminosities to dynamical evolution (accretion and cannibalism). The $r^{1/4}$ shape of all bright ellipticals is predicted by many theoretical studies of merger remnants, and suggests that all bright ellipticals ($M_V < -21$) may have at least one merger event in their past. At the very least, this change in structure signals the same change in the kinematics demonstrated by Davies *et al.* (1983).

Cluster properties yield ambiguous correlations with BCM luminosity, although the ranking test compares well with the evolution simulations of Malumuth and Richstone (1984). This problem, combined with the occurrence of cD galaxies which are not centrally located (e.g., NGC 6034 in Hercules), supports the hypothesis of Merritt (1984) that mergers were

important early in the life of a cluster, before virialization and the formation of a single cluster identity.

The author wishes to acknowledge the guidance of A. Oemler during the early stages of this project as a dissertation. This paper also benefited from conversations with J. Kormendy, D. Merritt, J. Tonry, and F. Schweizer. G. Bothun should be thanked for suggesting the morphology scheme based on profile shape. This project was partially supported by NSF grants AST 80-19986 and AST 84-16704.

REFERENCES

Arp, H. 1966, *Ap. J. Suppl.*, **14**, 1.
Bahcall, N. A. 1980, *Ap. J. (Letters)*, **238**, L117.
Bautz, L. P., and Morgan, W. W. 1970, *Ap. J. (Letters)*, **162**, L149.
Beers, T. C., and Geller, M. J. 1983, *Ap. J.*, **274**, 491.
Bertola, F., Gregg, M. D., Gunn, J. E., and Oemler, A. 1986, *Ap. J.*, **303**, 624.
Binggeli, B. 1982, *Astr. Ap.*, **107**, 338.
Binggeli, B., Sandage, A., and Tarenghi, M. 1984, *A.J.*, **89**, 64.
Caldwell, C. N., and Bothun, G. D. 1986, preprint.
Carnevali, P., Cavaliere, A., and Santangelo, P. 1981, *Ap. J.*, **249**, 449.
Cowie, L. L., and Hu, E. M. 1986, *Ap. J. (Letters)*, **305**, L39.
Davies, R. L., Efstathiou, G., Fall, S. M., Illingsworth, G., and Schechter, P. L. 1983, *Ap. J.*, **266**, 41.
de Vaucouleurs, G. 1948, *Ann. d'Ap.*, **11**, 247.
Djorgovski, S. 1985, Ph.D. thesis, University of California, Berkeley.
Dressler, A. 1976, Ph.D. thesis, University of California, Santa Cruz.
Duncan, M. J., Farouki, R. T., and Shapiro, S. L. 1983, *Ap. J.*, **271**, 22 (DFS).
Farouki, R. T., Shapiro, S. L., and Duncan, M. J. 1983, *Ap. J.*, **265**, 597 (FSD).
Forman, W., and Jones, C. 1982, *Ann. Rev. Astr. Ap.*, **20**, 547.
Gunn, J. E., and Tinsley, B. M. 1976, *Ap. J.*, **210**, 1.
Hausman, M. A., and Ostriker, J. P. 1978, *Ap. J.*, **224**, 320.
Hoessel, J. G., Gunn, J. E., and Thuan, T. X. 1980, *Ap. J.*, **241**, 486.
Hoessel, J. G., and Schneider, D. 1985, *A.J.*, **90**, 1648.
Holmberg, E. 1940, *Ap. J.*, **94**, 385.
King, I. R. 1966, *A.J.*, **71**, 64.
Kormendy, J. 1977, *Ap. J.*, **217**, 406.
_____. 1980, in Proc. ESO Workshop on Two-dimensional Photometry, p. 191.
Lauer, T. 1986, Ph.D. thesis, University of California, Santa Cruz.
Leir, A. A., and van den Bergh, S. 1977, *Ap. J. Suppl.*, **34**, 381.
Malin, D. F., and Carter, D. 1983, *Ap. J.*, **274**, 534.
Malumuth, E. M. 1983, Ph.D. thesis, University of Michigan.
Malumuth, E. M., and Kirshner, R. P. 1985, *Ap. J.*, **291**, 8.
Malumuth, E. M., and Richstone, D. O. 1984, *Ap. J.*, **276**, 413.
Matthews, T. A., Morgan, W. W., and Schmidt, M. 1964, *Ap. J.*, **140**, 35.
May, A., and van Albada, T. S. 1984, *M.N.R.A.S.*, **209**, 15.
Merritt, D. 1984, *Ap. J.*, **276**, 26.
_____. 1985, *Ap. J.*, **289**, 18.
Morgan, W. W., and Lesh, J. R. 1965, *Ap. J.*, **142**, 1364.
Oemler, A. 1976, *Ap. J.*, **209**, 693.
Ostriker, J. P., and Hausman, M. A. 1977, *Ap. J. (Letters)*, **217**, L113.
Pence, W. 1976, *Ap. J.*, **203**, 39.
Quinn, P. J. 1984, *Ap. J.*, **279**, 596.
Quintana, H., and Lawrie, D. G. 1982, *A.J.*, **87**, 1.
Romanishin, W. 1986, *A.J.*, **91**, 76.
Sandage, A. 1973, *Ap. J.*, **183**, 711.
Sastry, G. N. 1968, *Pub. A.S.P.*, **80**, 252.
Schneider, D. 1982, Ph.D. thesis, California Institute of Technology.
Schneider, D., Gunn, J. E., and Hoessel, J. G. 1983, *Ap. J.*, **268**, 476.
Schombert, J. M. 1984, Ph.D. thesis, Yale University.
_____. 1986, *Ap. J. Suppl.*, **60**, 603 (Paper I).
Schombert, J. M. 1987, in preparation.
Schombert, J. M., and Tonry, J. L. 1987, in preparation.
Schweizer, F. 1982, *Ap. J.*, **252**, 455.
Strom, K. M., and Strom, S. E. 1978*a*, *A.J.*, **83**, 73.
_____. 1978*b*, *A.J.*, **83**, 732.
_____. 1978*c*, *A.J.*, **83**, 1293.
_____. 1979, *A.J.*, **84**, 1091.
Struble, M. F., and Rood, H. J. 1986, preprint.
Thomsen, B., and Frandsen, S. 1983, *A.J.*, **88**, 789.
Thuan, T. X., and Gunn, J. E. 1976, *Pub. A.S.P.*, **88**, 543.
Thuan, T. X., and Romanishin, W. 1981, *Ap. J.*, **248**, 439.
Tonry, J. L. 1985, *A.J.*, **90**, 2431.
Toomre, A., and Toomre, J. 1972, *Ap. J.*, **178**, 623.
Valentijn, E., and Bijleveld, W. 1983, *Astr. Ap.*, **125**, 223.
Villumsen, J. V. 1982, Ph.D. thesis, Yale University.
White, S. D. M. 1982, Saas-Fée Lectures, p. 291.
Zwicky, F. 1964, *First Lists of Compact Galaxies, Compact Parts of Galaxies, Eruptive and Post-eruptive Galaxies* (Pasadena: California Institute of Technology).

JAMES M. SCHOMBERT: Palomar Observatory, California Institute of Technology, Mail Code 105-24, Pasadena, CA 91125